

# Accumulation rates and sources of sediments and organic carbon on the Palos Verdes shelf based on radioisotopic tracers ( $^{137}\text{Cs}$ , $^{239,240}\text{Pu}$ , $^{210}\text{Pb}$ , $^{234}\text{Th}$ , $^{238}\text{U}$ and $^{14}\text{C}$ )

Peter H. Santschi<sup>\*</sup>, Laodong Guo<sup>1</sup>, Shaunna Asbill, Mead Allison<sup>2</sup>,  
A. Britt Kepple, Liang-Saw Wen<sup>3</sup>

*Department of Oceanography, Laboratory for Oceanographic and Environmental Research, Texas A&M University,  
5007, Ave U, Galveston, TX 77551, USA*

Received 4 April 2000; received in revised form 21 September 2000; accepted 28 September 2000

---

## Abstract

We report here bioturbation and sediment accumulation rates determined from replicate sediment cores at four different sampling sites on the Palos Verdes shelf, Southern California, using bomb fallout and natural radionuclides ( $^{137}\text{Cs}$ ,  $^{239,240}\text{Pu}$ ,  $^{210}\text{Pb}$ ,  $^{234}\text{Th}$ , and  $^{14}\text{C}$ ), along with supporting measurements of organic carbon (OC), porosity and granulometry. Present-day particle reworking, on time scales of several months, is restricted to the upper 3 cm, with rates ranging from 13 to 200  $\text{cm}^2/\text{year}$ , as deduced from  $^{234}\text{Th}_{\text{xs}}$  profiles. There is little evidence that particle reworking reached depths significantly greater than 5 cm. Post-1963 (or post-1971) sediment accumulation rates ranged from 0.7 to 1.4  $\text{g}/\text{cm}^2/\text{year}$  (equivalent to 1.1–1.8  $\text{cm}/\text{year}$  for surficial sediments), as calculated from Pu and Cs isotope profiles, with little change over time or distance from the outfall. Lateral transport of older sediment and multiple sediment sources on the Palos Verdes shelf is suggested from radiocarbon measurements on foraminifera and bulk sedimentary organic matter at two sampling sites, which showed variable, old and refractory sources of OC. Pre-1953 sediments accumulated at rates that were at least 0.4  $\text{g}/\text{cm}^2/\text{year}$  ( $\geq 0.3 \text{ cm}/\text{year}$ ), based on  $^{210}\text{Pb}_{\text{xs}}$  dating. Given the abundance of sediment sources to the Palos Verdes shelf, the high sedimentation rates, and shallow particle mixed layers, contaminant-enriched layers should continue to move deeper into the sediments. © 2001 Elsevier Science B.V. All rights reserved.

*Keywords:* Sedimentation rates; Bioturbation; Sediment sources; Natural radionuclides; Fallout radionuclides; Palos Verdes shelf

---

---

<sup>\*</sup> Corresponding author. Tel.: +1-409-740-4476; fax: +1-409-740-4786.

*E-mail addresses:* santschi@tamug.tamu.edu (P.H. Santschi), guol@iarc.uaf.edu (L. Guo), malliso@mailhost.tcs.tulane.edu (M. Allison), lswen@odb03.gcc.ntu.edu.tw (L.-S. Wen).

<sup>1</sup> Present address: International Arctic Research Centre, University of Alaska, Fairbanks, AK 99750.

<sup>2</sup> Present address: Tulane University, Department of Geology, New Orleans LA 70118.

<sup>3</sup> Present address: National Centre for Ocean Research, National Taiwan University, Taipei, Taiwan, ROC.

## 1. Introduction

Continental shelves influenced by fluvial inputs often develop mid-shelf depocenters (e.g., Wheatcroft et al., 1997; Sommerfield and Nittrouer, 1999; Sommerfield et al., 1999). The Palos Verdes shelf in the Southern California Bight contains such a mid-shelf depocenter. Estimates of recent sedimentation rates near one particular site (6C) at 60 m water depth, however, range from a few mm/year to several cm/year (Emery, 1960; Logan et al., 1989; Farley, 1990; Drake et al., 1994; Wheatcroft and Martin, 1994; Niedoroda et al., 1996; Paulsen et al., 1999), partly due to differences in approaches and assumptions. Sediment sources to this depocenter include rivers, especially during floods, shore line, bluff and landslide toe erosion, primary production, and the Whites Pt. treated waste water outfalls, operated by the Los Angeles County Sanitation District. These outfalls have been in operation since 1937, and became a significant contributor of particle and pollutant loading in the early 1950s. A number of xenobiotics, such as DDTs, PCB's and heavy metals, were buried in shelf sediments adjacent to the outfalls (Bascom, 1982). With the introduction of strict nationwide regulations in the early 1970s, chemical fluxes from these outfalls decreased by one to two orders of magnitude, resulting in decreasing compound concentrations in the upper 30–50 cm of the sediments (Stull et al., 1996). Despite this burial, it is still feared that the higher concentrations of DDT present at depths of 30–50 cm will become a threat to the aquatic ecosystem (e.g., Drake et al., 1994; Niedoroda et al., 1996; Renner, 1998). For re-exposure to happen, accumulation of sediments would have to stop, and deep bioturbation and strong sediment resuspension would be required to bring DDT-laden particles back into the food chain of the water column. In order to assess such a possibility, a better knowledge of the rates of particle reworking and sedimentation, as well as sources of sediments on the Palos Verdes shelf, is required.

Not only is the rate of sedimentation or burial of these compounds still of great interest, but estimates of the natural (outfall-unaffected) sedimentation rates at one particular site (6C) on the Palos Verdes mid-shelf also vary by several orders of magnitude (e.g., Emery, 1960; Lee, 1994; Wheatcroft and Mar-

tin, 1994; Paulsen et al., 1999, and references therein; Eganhouse and Pontolillo, 2000). Some studies even concluded that recent sedimentation rates along the 60 m isobath should have dramatically decreased after the reduction in particle loading by the outfalls (Drake et al., 1994; Niedoroda et al., 1996), assuming that the Whites Point outfalls contributed a major fraction of sediments buried on the Palos Verdes shelf. The fraction of sediment directly contributed by these outfalls and deposited on the Palos Verdes shelf is, however, uncertain.

Using multiple isotopic tracers and replicate sediment cores, we obtained a detailed picture of sediment mixing and geochronology over a 10- to 100-year time scale. Sediment ages were determined from both bomb fallout ( $^{137}\text{Cs}$  and  $^{239,240}\text{Pu}$ ), and naturally occurring nuclides ( $^{210}\text{Pb}$ ,  $^{226}\text{Ra}$ ,  $^{234}\text{Th}$ ,  $^{238}\text{U}$ ). In addition, radiocarbon measurements were carried out on both bulk sedimentary organic carbon (OC) and foraminifera to study the apparent age and source distribution of sediments. These data were then used to obtain detailed estimates of bioturbation and sedimentation rates over the last 100 years.

## 2. Methods

Subcores from boxcores at sample sites 3C and 5C and a vibracore at site 3C were collected on October 22, 1996. In addition, a total of 11 boxcores were collected on September 17–18, 1997, at sites 6C and 8C, and one vibra core was collected at 6C. Subcores taken from the box cores, in which possible sub-coring artifacts were minimal (Santschi et al., 2000a), and vibra cores were sectioned on board ship, or on the same day on-shore. Coring and smearing artifacts were minimized by removing the outer rims from each slice before further processing. Sites 3C, 5C, 6C and 8C are 7, 3, 2 and 0 km from the outfall, respectively, and all are located at about 60 m water depth (Fig. 1 and Table 1).

Samples from all sediment cores were assayed in the laboratory, including the determination of  $^{234}\text{Th}$ ,  $^{137}\text{Cs}$ ,  $^{226}\text{Ra}$  and  $^{210}\text{Pb}$  (with lower precision) by gamma counting (Santschi et al., 1980, 1999), and the measurements of  $^{239,240}\text{Pu}$  and  $^{210}\text{Pb}$  were made

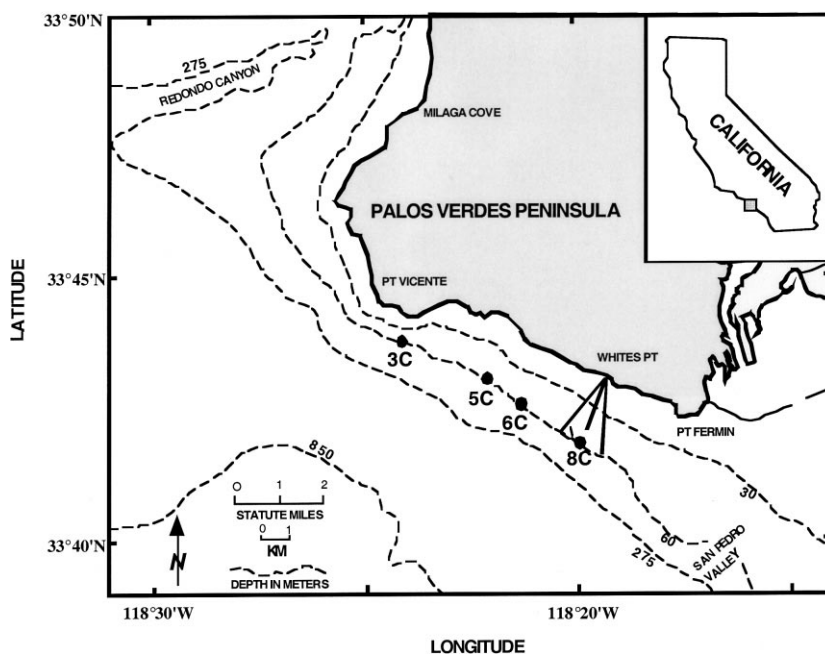


Fig. 1. Map of Palos Verdes shelf, showing sampling locations, and positions of Whites Point outfall pipelines.

by alpha counting (Santschi et al., 1980, 1999) after chemical extraction.

$^{210}\text{Pb}$  ( $t_{1/2} = 22.4$  year,  $E_{\gamma} = 46$  keV) was measured first by gamma counting of dried sediment samples of about 10 g each, followed by alpha counting after complete dissolution of 1 g aliquots in concentrated  $\text{HNO}_3$  and  $\text{HF}$  for  $^{210}\text{Pb}$  analysis, addition of  $^{209}\text{Po}$  tracer, chemical separation and spontaneous deposition of Po nuclides on Ag disks (Santschi et al., 1980, 1999; Ravichandran et al., 1995a,b).  $^{234}\text{Th}$  ( $t_{1/2} = 24.1$  days),  $^{226}\text{Ra}$  ( $t_{1/2} = 1600$  year),  $^{137}\text{Cs}$  ( $t_{1/2} = 30$  year) were measured by gamma counting at  $E_{\gamma} = 63, 351,$  and  $662$  keV, respectively.  $^{239,240}\text{Pu}$  ( $t_{1/2} = 2.41 \times 10^4, 6.57 \times 10^3$  year) was measured by alpha counting, after digestion of 10 g dried sediment in 6 M  $\text{HCl}$  and 8 M  $\text{HNO}_3$ , addition of  $^{242}\text{Pu}$  tracer, chemical separation and electroplating onto stainless steel disks.

Gamma counting was carried out in a low-background, high-efficiency high-purity Germanium (HPGe) well detector (Canberra) for at least 1 day. Alpha counting of samples was carried out on surface barrier detectors (Canberra) for 3–4 days to reach a standard deviation of  $\leq 3$ –5%. Supported

$^{210}\text{Pb}$  was determined from the average of  $^{210}\text{Pb}(\text{total})$  activities in deeper sections of the vibra cores, measured by alpha counting, which were constant within the errors of the measurements. The constancy of  $^{226}\text{Ra}$ -supported  $^{210}\text{Pb}$  activities was verified by measurements of  $^{226}\text{Ra}$  activities by gamma counting.

Supported  $^{234}\text{Th}$  activities were determined from average activities in layers at 5–10 cm depth, and by recounting surface samples after 4–5 months. No corrections for self-absorption of the low energy gamma peaks of  $^{234}\text{Th}$  and  $^{210}\text{Pb}$  needed to be applied since the sediment density in the counting vials was close to the density of the liquid standards used to calibrate the detectors. Correction factors were determined to be significantly less (i.e.,  $< 2\%$ ) than the counting error.

$^{137}\text{Cs}$ ,  $^{234}\text{Th}_{\text{xs}}$  and  $^{210}\text{Pb}_{\text{xs}}$  concentrations were considered to be significant only when they were greater than about 3 standard deviations of the propagated counting errors (Adloff and Guillaumont, 1993). Such a criterion results in a significance level of 96%, given that the total activity,  $A_1 = N_1/t_1$ , needs to be higher than the “background” or “sup-

Table 1

Summary of sedimentation and mixing parameters, resulting from this work. Errors are those calculated from numerical modeling, linear regression analysis, or from relative peak position

Site/ core <sup>a</sup>	Porosity ( $\phi$ )			Sedimentation rate <sup>b</sup> (cm/year) ( $\pm 1\sigma$ )		Accumulation rate <sup>b</sup> (g cm <sup>2</sup> /year) ( $\pm 1\sigma$ )		Bioturbation rate (cm <sup>2</sup> /year) ( $\pm 1\sigma$ ) <sup>c</sup>	Thickness (cm) ( $\pm 1\sigma$ )
	Surface	Max	Min	Recent	Long-term	Recent	Long-term	Surface	Surface mixed layer
8C	0.70	0.80	0.70	1.1	–	0.75	–	–	–
6C	0.70	0.78	0.70	1.3	–	0.90	–	13, 159, 178 ( $\pm 249$ )	3 $\pm$ 1
6CV	0.70	0.80	0.50	1.3	0.30 (+0.3, –0.1)	0.90	0.40 (+0.40, –0.13)	–	–
5C	0.70	0.78	0.50	1.52 $\pm$ 0.03	0.3 (+0.05, –0.04)	1.09 $\pm$ 0.03	0.4 (+0.07, –0.05)	33 $\pm$ 2	3 $\pm$ 1
3C	0.65	0.65	0.50	0.97 $\pm$ 0.03	–	0.92 $\pm$ 0.03	–	18	2 $\pm$ 1
3CV	0.68	0.65	0.47	1.06 $\pm$ 0.03	0.35 (+0.13, –0.08)	0.96 $\pm$ 0.03	0.44 (+0.16, –0.10)	39	2 $\pm$ 1

<sup>a</sup>Core locations (and water depths) are: 8C: 33°42.00N; 118°20.05S (56 m); 6C: 33°42.51N; 118°21.20S (59 m); 5C: 33°42.91N; 118°21.90S (58 m); 3C: 33°43.84N; 118°24.13S (58 m).

<sup>b</sup>Recent means here post-1953, and long-term means pre-1953.

<sup>c</sup>Calculated from  $\Delta D_b = 1\sigma \times (2\lambda/b^3)$ , with  $1\sigma$  = standard error of the regression coefficient,  $b = (\lambda/D_b)^{1/2}$  (Wheatcroft and Martin, 1996).

ported" activity,  $A_2$ , by  $x\sqrt{(2N_2)}/t_2 = 2.8$  sigma- $A_2$ , at  $x =$  number of standard deviations = 2 (96% significance level) or  $x = 3$  (99.9% significance level);  $N_2 =$  number of background counts,  $t_2 =$  counting time for background. Repeated activity determinations of samples which should have had zero activity confirmed such a criterion for the detection limit (e.g.,  $^{137}\text{Cs}$  in Table A3, 3C(VC) core). Due to a slightly contaminated acid bath during the processing of 6C samples, Pu data needed to be corrected for a blank level equivalent to  $4 \pm 2$  dpm/kg. Blanks were below the detection limit for all other samples.

Radiocarbon in sedimentary OC and foraminifera was measured by Accelerator Mass Spectrometry (AMS, McNichol et al., 1994), after sediments were sieved and sorted for benthic (*Quinqueloculina* sp.) and planktonic (*Globigerina*) foraminifera, to be compared with those of bulk sedimentary OC.

The total number of sediment samples for radiochemical determinations was over 200, with over 100 determinations for  $^{239,240}\text{Pu}$  and  $^{210}\text{Pb}$  by alpha counting, over 200 for  $^{234}\text{Th}$  and  $^{137}\text{Cs}$  by gamma counting, 13 for  $^{14}\text{C}$  in OC, and 10 for  $^{14}\text{C}$  in foraminifera by AMS. 10–20% of the samples were normally measured in duplicates, and 27 samples were recounted after short-lived  $^{234}\text{Th}_{\text{xs}}$  had decayed away in order to verify the  $^{238}\text{U}$  supported  $^{234}\text{Th}$  values. Blanks were determined for all nuclides using all reagents and procedures. Detectors were calibrated using NIST or NIST-traceable standards.

X-Radiography from sites 6C, 8C was carried out on-board ship, while that from site 5C were carried out later in the lab. Plexiglass ( $10 \times 4 \times 90$  cm) tray cores were pushed into box cores, and X-rayed with a Kramex PX-20N machine at 15 mA/70 kV. Fuji sheet negatives were developed on board and later

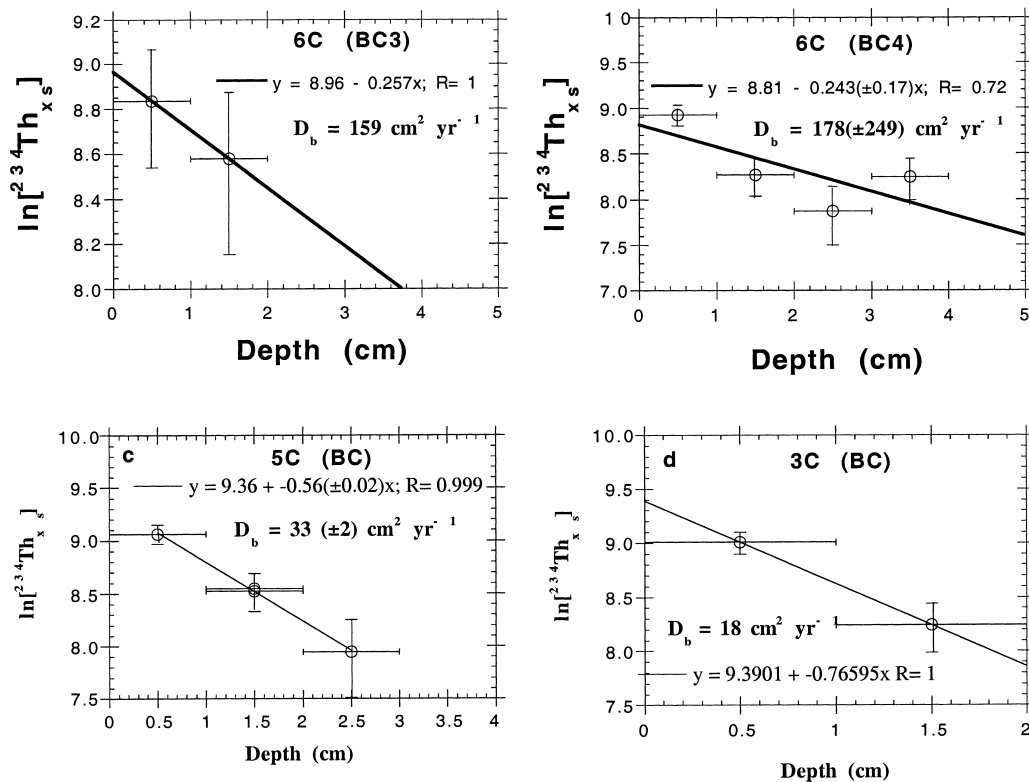


Fig. 2. Examples of  $^{234}\text{Th}_{\text{xs}}$  ( $= [^{234}\text{Th}(\text{total})] - [^{238}\text{U}]$ ) penetration into surface sediments from sites 6C, 5C and 3C allowing determination of particle reworking (bioturbation) rate ( $D_b$ ) and depth ( $z_m$ ). Units are in dpm/kg. Only points with values which exceed three times the propagated  $1\sigma$  error have been considered as significant.  $D_b$  was calculated from the slope of  $\ln[^{234}\text{Th}_{\text{xs}}(z)] = \ln[^{234}\text{Th}_{\text{xs}}(0)] - (\lambda/D_b)^{1/2}z$ .

scanned into digital form at 300 dpi resolution. Individual X-ray sections of cores were merged digitally to form a single image of each core.

Additional analyses included those for OC, total nitrogen (Hedges and Stern, 1984; Guo and Santschi, 1997), grain size (Folk, 1968; Santschi et al., 1999; Drake and Eganhouse, 1994), and trace metals. Trace metal results are presented elsewhere (Santschi et al., 2000b).

A description of the one-dimensional mixing and sedimentation model used in this study can be found in Santschi et al., (1980, 1999).

### 3. Results and discussion

Results of radiochemical determinations are tabulated in Appendix A (Tables A1–3). These data are used to calculate particle reworking (bioturbation) and sedimentation rates in these sediments discussed in detail below.

#### 3.1. Bioturbation rates

Bioturbation rates can be quantitatively derived from  $^{234}\text{Th}_{\text{xs}}$  profiles according to Santschi et al. (1980, 1999), from the analysis of peak shapes of different tracer concentration profiles, and qualitatively from X-radiography profiles.  $^{234}\text{Th}_{\text{xs}}$  profiles, calculated as the difference between  $^{234}\text{Th}(\text{total})$  and supported  $^{234}\text{Th}$  ( $^{234}\text{Th}_{\text{supp}} = ^{238}\text{U}$ ), were used to determine the particle reworking (or bioturbation) rate coefficients,  $D_b$ , displayed in Fig. 2, which, assuming steady state conditions, were calculated as follows:

$$[^{234}\text{Th}_{\text{xs}}(z)] = [^{234}\text{Th}_{\text{xs}}(0)] \exp(-(\lambda/D_b)^{1/2} z) \quad (1)$$

where  $\lambda$  = decay constant of  $^{234}\text{Th}$  ( $0.0288 \text{ day}^{-1}$ );  $z$  = depth (cm).

$^{234}\text{Th}_{\text{supp}}$  concentrations in all sediment cores slightly increase with depth in the upper 0–20 cm (Appendix A, Table A1; and Fig. 3). Below 20–30

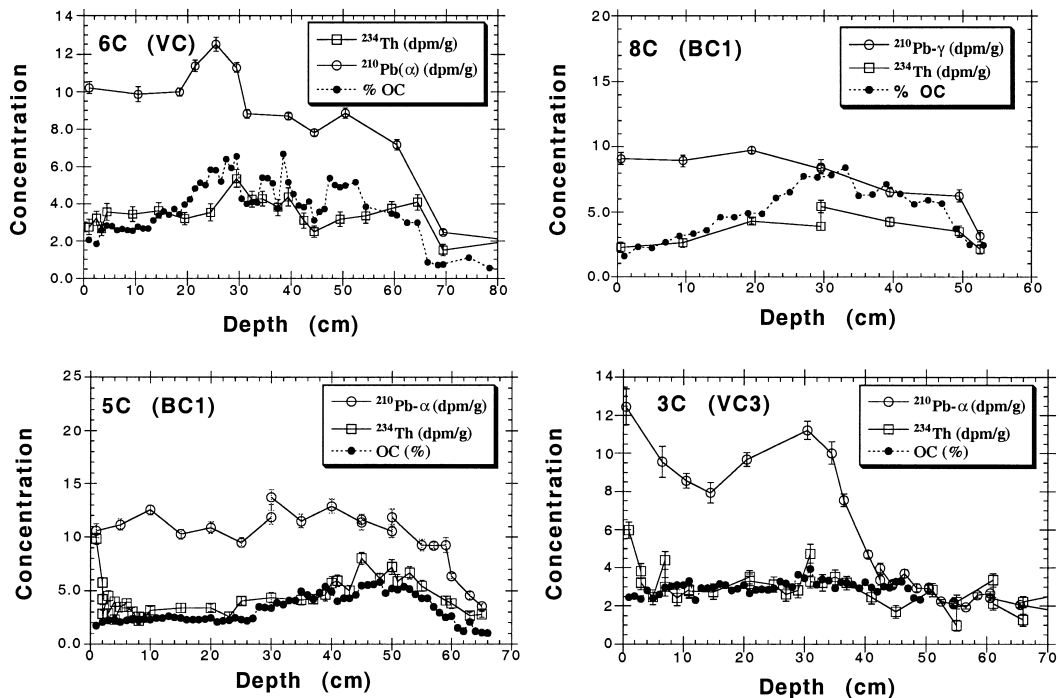


Fig. 3. Representative profiles of  $^{210}\text{Pb}_{\text{xs}}$  ( $= [^{210}\text{Pb}(\text{total})] - [^{210}\text{Pb}(\text{supported})]$ ) and total  $^{234}\text{Th}$  (which is in equilibrium with  $^{238}\text{U}$  below about 3–5 cm depth) in sediments from site 6C, 8C, 5C and 3C, compared to organic carbon (OC) profiles. Values which are less than  $3\sigma$  error of the baseline (i.e., supported activity) are not shown.

cm depth, they increase more sharply to a subsurface peak, an effect caused by the outfall which will be discussed later. As shown in Fig. 2 and Table 1,  $^{234}\text{Th}_{\text{xs}}$  penetration depths are about 2–4 cm at all sites, and bioturbation coefficient values,  $D_b$ , range from 13 to 200  $\text{cm}^2/\text{year}$ , with relatively high errors.  $D_b$  values are in the range of those reported for sites 3C and 6C by Wheatcroft and Martin (1996), and are somewhat higher than those used by Logan et al. (1989) to model their  $\Sigma\text{DDT}$  profiles. Paulsen et al. (1999) successfully modeled profiles, assuming instantaneous mixing over a shallow depth (1–3 cm). Thus, when judging an average  $D_b$  value, one must also consider the depth dependence of  $D_b$ , as model-derived average  $D_b$  values depend on the assumed values for the mixing depth. Our values for mixing depths are in good agreement with the low values required by model simulations of profiles of  $\Sigma\text{DDT}$  by Logan et al. (1989) and trace metals by Paulsen et al. (1999), as well as those determined by Wheatcroft and Martin (1994, 1996) using  $^{234}\text{Th}_{\text{xs}}$  penetration, when their data sets are evaluated using the same  $3\sigma$  error criterion.

Because particle reworking (bioturbation) rates can be expected to decrease exponentially with depth, in accordance with the depth distribution of benthic infauna (Stull et al., 1996; Wheatcroft and Martin, 1996), it is unlikely that the depth of more intensively mixed sediments is much higher than observed by  $^{234}\text{Th}_{\text{xs}}$  data. Test runs by the numerical mixing and sedimentation models (see below) demonstrate that the constant  $D_b$  model is conservative in the sense that it tends to overpredict mixing rates and mixed layer depth. Applying non-linear curve-fitting procedures to the data did not change that conclusion. While our  $^{234}\text{Th}_{\text{xs}}$  data, due to limited penetration depths, do not allow us to investigate the issue of a decreasing  $D_b$  value with depth any further, the data of Wheatcroft and Martin (1996) from a site near 6C are better suited to illustrate this point. An example, given in Fig. 4, shows that some of the  $^{234}\text{Th}$  data from Wheatcroft and Martin (1996) can indeed fit better with a model that assumes  $D_b$  to decrease exponentially with depth, i.e., assuming  $D_b(z) = D_b(0)\exp(-\alpha z)$ , with  $\alpha = 0.3 \text{ cm}^{-1}$ . Thus,  $D_b$  would decrease by more than an order of magnitude over the top 8 cm. With  $D_b(z) = D_b(0)\exp(-\alpha z^2)$ , as suggested by others (e.g.,

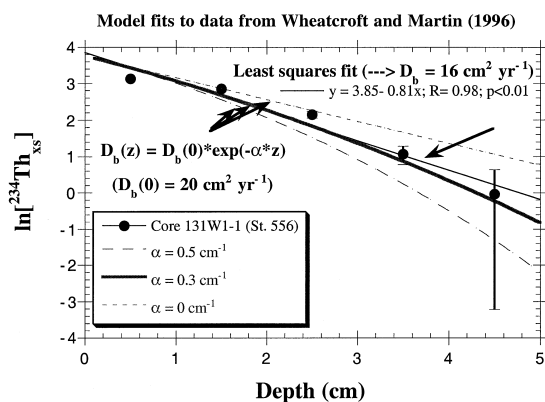


Fig. 4. Comparison of model profiles to the data of Wheatcroft and Martin (1994) using depth variable or depth invariant  $D_b$  values.

Niederoda et al., 1996),  $D_b$  would decrease even faster with depth.

A decreasing  $D_b$  value with depth is also suggested by the discrepancy at this site (Wheatcroft and Martin, 1996) between the gradient method, as was also used here, and Aller's inventory method. The Aller method assumes that  $D_b$  is constant over the top 5 cm, and calculates  $D_b$  from the ratio of the  $^{234}\text{Th}_{\text{xs}}$  activity in the top 1 cm to the average activity in the top 5 cm. Any activity concentration below 1 cm, which is higher than the least-square fit line would predict, as would be true in the case of an exponentially decreasing  $D_b$  (Fig. 4), would result in a higher average activity in the upper 5 cm, and thus, a higher estimate of  $D_b$  than the gradient method. No evidence for mixing below 7 cm depth was evident from our tracer data (Appendix A, Table A1); even when only  $1\sigma$  errors were considered. However, an average mixed layer thickness of 7 cm, as a yearly average, is not consistent with measured tracer profiles. For example, profiles of trace metals (Paulsen et al., 1999), DDTs (Logan et al., 1989), and the  $^{239,240}\text{Pu}$  profile at 3C (discussion below) can only be modeled with a mixed layer depth which is close to the 3 cm we determined here. The extent of bioturbation described here is also consistent with the macrofauna distribution reported by Wheatcroft and Martin (1996). These authors found the majority of their benthic infauna specimens to be concentrated in the uppermost layers of the sediment. For example, 40–60% was in the 0–2 cm, 20–35% in the 2–4 cm, and 10–15% in 4–8 cm layers. Animal abun-

dance was extremely low in their 8–20 cm interval. As a consequence of this shallow mixed layer depth, sediment is anoxic below about 2 cm, and  $H_2S$  is easily measurable up to the sediment surface (Carry, 1996; Van Cappellen et al., 2000).

Within the region of high concentrations of radionuclides and OC, there are narrow sub-peaks

(Fig. 5). From the peak width at half of the maximum concentration (also called “Full Width at Half Maximum” = FWHM =  $\Delta X$ ), one can estimate an upper limit of the bioturbation rate at the time of deposition, assuming (1) an input that only occurred over a short time scale; (2) a constant sedimentation rate; and (3) that peak broadening is only caused by

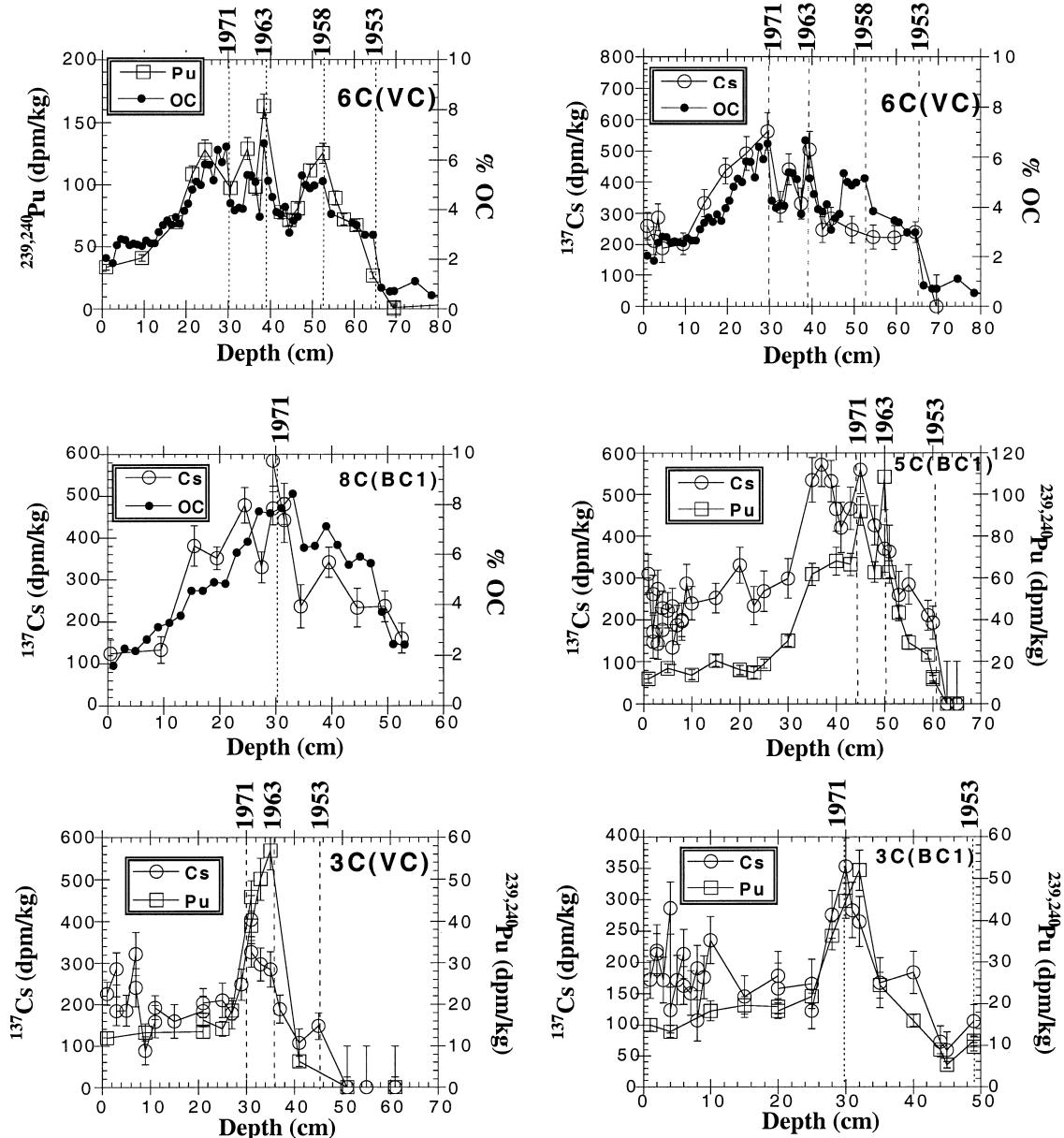


Fig. 5. Examples of  $^{239,240}\text{Pu}$ ,  $^{137}\text{Cs}$  and organic carbon (OC) profiles used to assign dates to site 6C, 8C, 5C and 3C cores.

mixing over the time the tracer resides in the surface mixed layer. Typical values for the FWHM are 6 cm (Fig. 5), which is twice our measured average mixed layer depth of about 3 cm (Fig. 2). With a typical sedimentation rate of 1.5 cm/year, the average time ( $\Delta t$ ) for passage of a tracer through the mixed layer would thus be about 2 years, in agreement with numerical modeling of metal and  $^{210}\text{Pb}_{\text{xs}}$  profiles (Paulsen et al., 1999). Given that:

$$\Delta X = 3.3(D_b \Delta t)^{1/2} \quad (2)$$

where  $D_b$  = particle reworking or bioturbation rate (Robbins et al., 1979),  $D_b$  can then be calculated as:

$$\begin{aligned} D_b &= (1/\Delta t)(\Delta X/3.3)^2 \\ &= (1/2 \text{ year})(3 \text{ cm}/3.3)^2 = 0.4 \text{ cm}^2/\text{year}. \end{aligned}$$

The value of  $D_b$  estimated here is an upper limit. If tracer mixing or tracer input had occurred over much longer periods than assumed here (e.g., 26 years), the  $D_b$  value one would calculate would be even lower.  $D_b$  values of  $\sim 0.4 \text{ cm}^2/\text{year}$  are considerably lower than the present-day values determined at site 6C in 1997 (10–200  $\text{cm}^2/\text{year}$ ), and at sites 3C and 5C in 1996 (20–30  $\text{cm}^2/\text{year}$ ; Table 1 and Fig. 2). These seemingly contradictory observations can be reconciled if sedimentation rates were significantly higher than average during burial of these features. This would suggest episodic deposition events.

Because of episodic effects by lateral (cross-shelf exchange) deposition of different particle assemblages (see further discussion below), a process that is not included in the simple one-dimensional mixing and sedimentation model (Santschi et al., 1980, 1999; Crusius, 1992), it was only possible to simulate one of the  $^{239,240}\text{Pu}$  profiles (site 3C), using measured sedimentation and mixing parameters and a bomb fallout input function (Fig. 6). Even at 3C, which is 7 km away from the outfall, however, the predicted peak shape (width) is too broad, and only when smaller values for the particle mixing rates and depths (e.g., 3 cm) were assumed could the narrow Pu peak be more closely matched. The Pu concentrations near the sediment surface that are higher than predicted by the model are due to additional inputs from the water and land (Santschi et al., 1999; Wan et al., 1987; Van Metre et al., 1998; Oktay et al., 2000), which were not considered by the model.

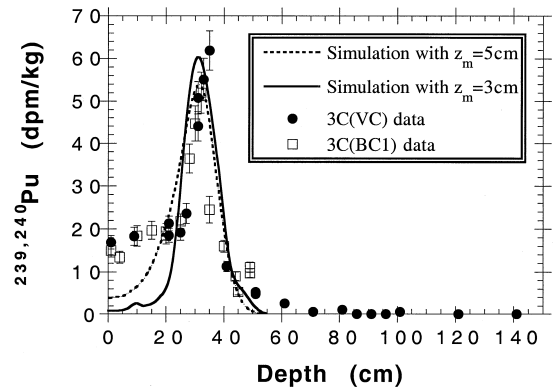


Fig. 6. Example of a numerical simulation of a  $^{239,240}\text{Pu}$  profile in 3C sediments using measured (5 cm) and low mixing depth (3 cm). The values near the surface, which are not predicted well by the model, are caused by the fact that contemporary terrestrial and marine particles still contain substantial amounts of  $^{239,240}\text{Pu}$ , an input which is not simulated by the model.

Such model calculations are nonetheless useful since they confirm a number of assumptions about the tracer peak position in the sediments. For example, it confirmed that the magnitude of downward displacement of the peak position by particle mixing effects is small. Overall, however, simple model simulations assuming only a single source of sediments and tracers for these sites are precluded by the multiple sources of fine-grained sediments to the Palos Verdes shelf, which are likely responsible for the multiple peaks at sites 5C, 6C and 8C (see discussion above).

X-radiographs provide another qualitative measure of bioturbation intensity. An example of an X-radiography profile is shown in Fig. 7a. Note that the sharp division at about 30 cm in the X-radiograph picture is the result of piecing together the whole section from separate films. The observations from six usable X-radiographs taken at sites 6C and 8C can be summarized as follows.

(1) The two sites, 6C and 8C, have very similar stratigraphy.

(2) Cores show evidence of strong surface bioturbation with no continuous physical stratification preserved. However, there is a surface layer of lower X-ray penetration (e.g., higher specific gravity), indicating that bioturbation is not sufficient to make cores appear massive in fabric. Generally the cores appear mottled (discontinuous laminations preserved), particularly below the surface layer.

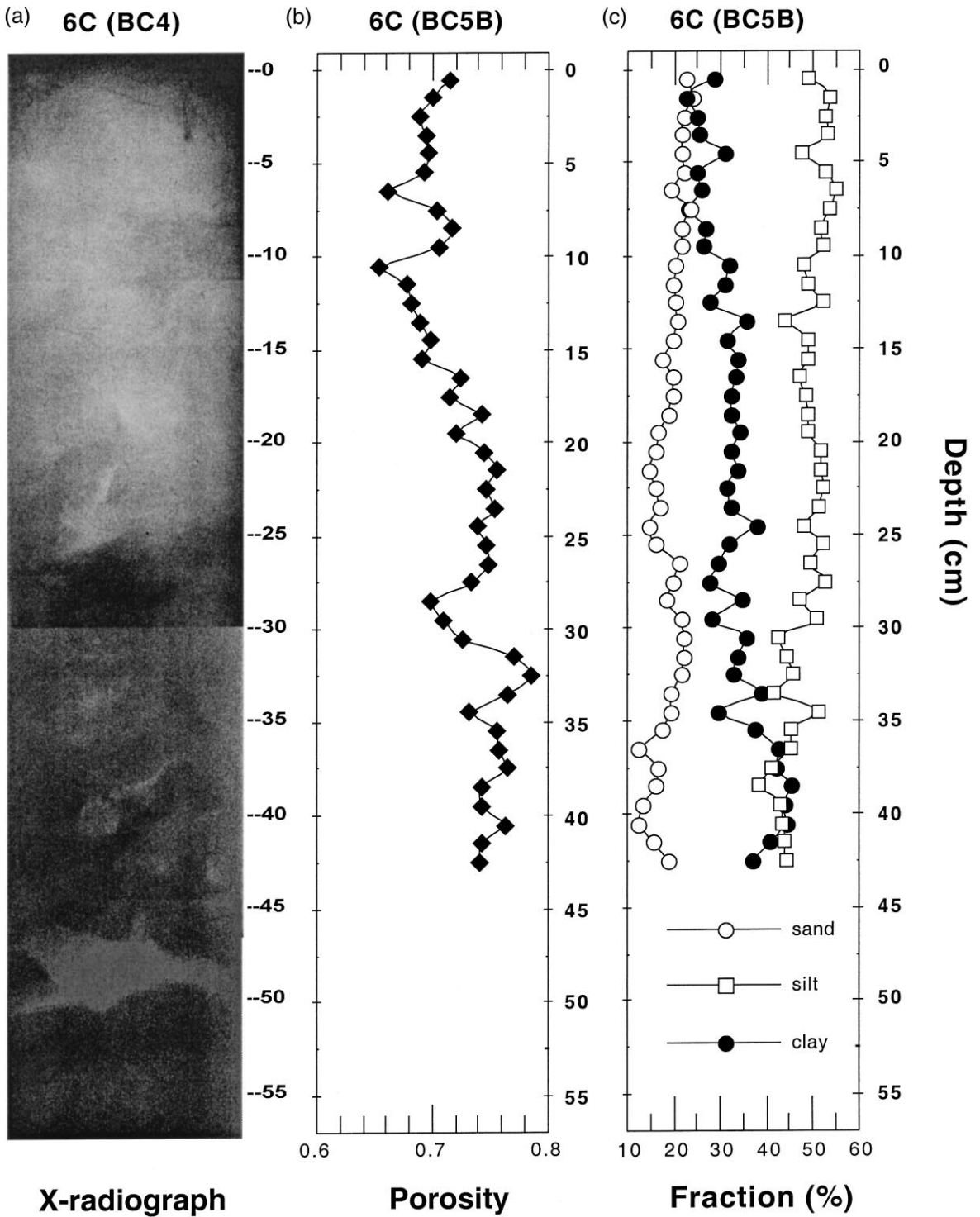


Fig. 7. An example of profiles of (a) X-radiography, (b) porosity and (c) size distribution at site 6C.

(3) The sandier and denser surface layer is 18–25 cm thick in 8C and 15–24 cm thick in 6C, which agrees with the depth of the lower porosity layer near the sediment–water interface. This sandy layer overlays a layer of higher porosity (i.e., effluent sediments, see Fig. 7b).

(4) Recently, active burrows are occasionally preserved on the otherwise mottled surface. Most are on the present seabed surface and extend to < 5 cm depth. The only two burrows identified below the surface mixed layer (out of six X-radiographs) are 5–12 cm long and extend to 15 cm depth. However, they are relics because they are lined with sandier sediments and have not been reworked.

(5) A zone from about 20–40 cm sometimes shows remnants of large diameter (3 cm) burrows backfilled with sandier material. Only one relatively complete burrow (15 cm long) was noted, which was at site 5C, but it did not extend into the more recent sediments (e.g., < 20 cm). This could have been caused by the echiuran *Listrolobus pelodes*, which was abundant in these sediments between 1974 and 1978 (Stull et al., 1986).

### 3.2. Sedimentation rates

#### 3.2.1. Recent sedimentation rates

Short-term sedimentation rates can, in principle, be derived from the relative peak positions of fallout nuclides (Santschi et al., 1980, 1999; Ravichandran et al., 1995a,b; Santschi and Honeyman, 1989). Despite the fact that both  $^{137}\text{Cs}$  and  $^{239,240}\text{Pu}$  significantly correlate with OC ( $R > 0.9$ ,  $n = 20\text{--}37$ ), they have lower correlation coefficient values ( $R$ ) than those for trace metals in the same cores (Santschi et al., 2000b). Profiles of  $^{137}\text{Cs}$  and  $^{239,240}\text{Pu}$  (Fig. 4) show slightly different peak positions, suggesting that Cs and Pu were not always deposited at a constant ratio in these sediments. However, the major  $^{239,240}\text{Pu}$  peak always occurred below that of  $^{137}\text{Cs}$  at these sites, and can therefore be reliably assigned to the year 1963 when bomb fallout deposition peaked. Sediment dating was therefore mainly based on the 1963 peak position of the more particle-reactive, and thus more reliable,  $^{239,240}\text{Pu}$ .

The  $^{137}\text{Cs}$  profile, in general, closely matches that of OC, suggesting that Cs concentrations also peaked in 1971, when sedimentation and OC deposition rates peaked in the sediments, rather than in 1963.

This peak displacement of Cs is unexpected for nuclides mainly derived from atmospheric fallout, as both Cs and Pu nuclides were deposited in relatively constant ratios to the earth surface.

Furthermore, Pu/Cs concentration ratios in sediments are enhanced by about an order of magnitude over fallout ratios. This apparent concentration enhancement of particle-reactive Pu over the more soluble Cs could be explained by the same effect by which the outfall-derived sedimentation enhanced the concentration and deposition rate of the particle-reactive  $^{210}\text{Pb}$  (Paulsen et al., 1999). In addition to this outfall-derived enhanced scavenging and deposition effect, concentrations of atmospherically delivered nuclides in suspended particles of the water column could also have been enhanced by nuclide inputs from the outfall, or from surface runoff during the 1960s, similar to the situation during the much better documented Chernobyl fallout (Santschi et al., 1988, 1990). Fractionation processes in soils, in sewage treatment plants, during surface runoff, or in the water column, could be reasons why the  $^{137}\text{Cs}$  maximum always coincides with the OC maximum, while the  $^{239,240}\text{Pu}$  maximum is always found below that depth. When  $^{137}\text{Cs}$  is decay-corrected to the time of deposition using the Pu-derived geochronology, however, its profiles more closely match those of  $^{239,240}\text{Pu}$  (Fig. 8). Such a decay correction would be justified when there is a time delay between the movement from source (e.g., surface water and surface soil receiving atmospheric deposition) to sink (e.g., sediments). It is frequently applied to profiles of radioisotopes in environmental archives such as sediments to make them comparable to long-lived and stable tracer profiles (e.g., Wan et al., 1987; Van Metre et al., 1998; Oktay et al., 2000).

As a result of these observations, we used the following isotopic tracers to mark the positions for the years 1971, 1963, 1958 and 1953, as shown in Fig. 4.

1971: Peak in  $^{137}\text{Cs}$ ,  $^{234}\text{Th}$  (total), OC, and sometimes in  $^{210}\text{Pb}$  concentrations; the peak in OC and tracer emissions in 1971 was already used in previous studies to assign observed OC and tracer maxima to that year (e.g., Logan et al., 1989; Stull et al., 1996; Paulsen et al., 1999); in agreement with this approach, trace metal (Galloway, 1972; Young et al., 1975), OC (Myers, 1974; Eganhouse and Kaplan,

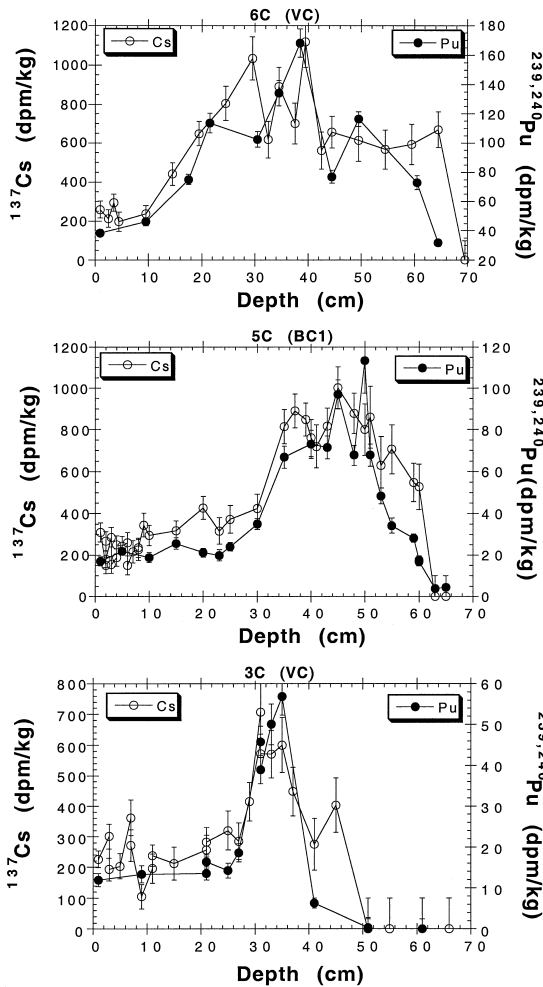


Fig. 8. Comparison of  $^{239,240}\text{Pu}$  with  $^{137}\text{Cs}$  (decay-corrected to the time of deposition) profiles used to assign dates to selected sites 6C, 5C and 3C cores.

1982) and DDTs (Eganhouse and Kaplan, 1982) concentration profiles in sediment cores taken in 1972 and 1971 showed concentration maxima at the surface.

1963: Peak in  $^{239,240}\text{Pu}$  concentration.

1958: Minor peak in  $^{239,240}\text{Pu}$  concentration below that of 1963, with significant differences to OC and Cs profiles.

Pre-1953:  $^{239,240}\text{Pu}$  (or  $^{137}\text{Cs}$ ) activity concentrations below the detection limit.

Using this approach, sedimentation rates at the different sites could be calculated for specific time intervals (Table 2). Such an approach, of course,

assumes minimal disturbance of the original sedimentary record by particle reworking (bioturbation) effects. This assumption is justified by the modest mixed layer depths of 2–4 cm (Table 1) observed at all sites (equivalent to 1–3 years of sedimentation), and the sedimentation and bioturbation studies of Logan et al. (1989) and Paulsen et al. (1999). As discussed above, mixed layer depths had to be even lower in the 1960s and early 1970s, given the sharp peaks, and given the fact that  $^{210}\text{Pb}$  and trace metal profiles from all the sites can consistently be modeled only when mixed layer depths are assumed of a thickness that is not more than one to two years worth of accumulated sediment (Paulsen et al., 1999). The comparison of our sedimentation rate data in Table 2 show that (1) there is no discernible pattern in inferred sedimentation rates over time or distance; (2) different sites have received about the same average amount of sediments since the 1950s; and (3) maximum inferred sedimentation rates are found at different times by the same or different investigators at close-by sites.

Average calculated sedimentation rates at different sites (Tables 1 and 2) are generally over 1 cm/year. This corresponds to a recent sediment accumulation rate of over  $0.8 \text{ g cm}^{-2}/\text{year}$ . In many cores, however, the highest sedimentation rates occurred in the most recent time interval (e.g., our 5C core, and in a core taken near 3C, see Eganhouse, 1996). Therefore, there is no indication of any decrease in sedimentation rates in more recent times, which would be expected, if most sediment originated from the outfall. In the contrary, sedimentation rates in the last two decades appear to have increased, as was also reported by Eganhouse and Pontolillo (2000). In our data, the relatively large variation of estimated short-term sedimentation rates in different time periods in one core from one site is not replicated in another core. However, our average post-1953 sedimentation rate estimates at the different sites appear to be quite uniform, and are in close agreement with a number of other determinations, as summarized in Table 2.

Dating techniques, which are based on time markers, such as bomb fallout radionuclides, provide only average sedimentation rates, and no information on very recent sedimentation rates. In order to estimate current sedimentation rates, other approaches are

Table 2  
Comparison of recent sedimentation rates in Palos Verdes shelf sediments

Site (core)	Period	Sedimentation rate (cm/year)	Sediment accumulation rate (g/cm <sup>2</sup> /year)	Method	Author
3C(VC)	1900–1953	0.35 (+0.13, –0.08)	0.44	<sup>210</sup> Pb <sub>xs</sub> <sup>239,240</sup> Pu maxima <sup>239,240</sup> Pu, <sup>137</sup> Cs and OC maxima	This work
	1953–1963	1.3	1.35		
	1963–1971	0.9	0.8		
3C(BC)	1971–1997	1.2	1.05		This work
	1953–1971	1.1	1.25		
5C(BC1)	1971–1996	1.2	1.1	<sup>239,240</sup> Pu maxima <sup>239,240</sup> Pu, <sup>137</sup> Cs and OC maxima	This work
	1953–1963	1.0	0.9		
6C(BC4)	1963–1971	0.6	0.5	<sup>239,240</sup> Pu maxima <sup>239,240</sup> Pu, <sup>137</sup> Cs and OC maxima	This work
	1971–1996	1.8	1.4		
	1953–1963	1.2	0.75		
6C(VC)	1963–1971	1.4	0.8	<sup>239,240</sup> Pu, <sup>137</sup> Cs and OC maxima, Cu/Zn minima	This work
	1971–1997	1.3	0.9		
	1913–1953	0.3 (+0.3, –0.1)	0.38		
	1953–1958	2.0	1.6		
	1958–1963	3.0	1.9		
	1963–1971	1.1	0.75		
8C(BC1)	1971–1997	1.1	0.75	modeling of pore water and TS data	Calculated from Van Cappellen et al. (2000)
	1997	–	0.9		
3C	1953–1971	1.3	0.9	<sup>137</sup> Cs and OC maxima	This work
	1971–1997	1.2	0.7		
3C	1955–1965	0.9	1.1	Biomarker maxima (LAS <sup>a</sup> , etc.)	Eganhouse and Pontolillo (2000)
	1965–1971	1.3	1.4		
	1971–1981	0.8	0.9		
	1981–1992	2.1	2.2		
3C	1951–1971	0.7	–		Eganhouse and Kaplan (1988)
	1971–1972	2.0	–		
	1971–1981	0.7	–		
	1964–1981	0.8	–		
6C	1985	~ 2.0	0.7–0.8	modeling OC and DDTs data	Logan et al. (1989)
6C	1989	2.5	–	modeling OC data	Farley (1990)

<sup>a</sup>LAS = Linear alkyl sulfonates.

needed. For example, one can compare the integrated sulfate reduction rate (SR) and total sulfur burial rate near the sediment surface, which should balance each other if most of the carbon oxidation is occurring through sulfate reduction, and all sulfur is pro-

duced locally. The integrated sulfate reduction rate at site 6C, calculated from a diagenetic model simulation of pore water data (oxygen microelectrode, sulfate, hydrogen sulfide, pH microelectrode, alkalinity, nitrate, ammonia, Fe, Mn), is about 300 μmol

cm<sup>2</sup>/year (Van Cappellen et al., 2000). Our measured total sulfur concentration ([S]) in the upper 1–10 cm is 1.0–1.1% (Santschi et al., 2000b), with > 90% of this representing reduced sulfur.

Therefore,  $SR = [S] \times S_a$ , where  $S_a$  = sediment accumulation rate, in g cm<sup>2</sup>/year. Using values for SR and [S] given above,  $S_a$  becomes 0.9 g/cm<sup>2</sup>/year, which is very similar to the value derived from radionuclide tracers (Table 2). While this agreement could be coincidental, since the assumptions have not been rigorously tested, it is encouraging.

It is also interesting to note that in the close vicinity of the depth assigned to the year 1971, subsurface maxima not only occur for OC, but also for <sup>210</sup>Pb<sub>xs</sub> and total <sup>234</sup>Th, <sup>234</sup>Th<sub>t</sub> (in equilibrium with <sup>238</sup>U, i.e., [<sup>234</sup>Th<sub>t</sub>] = [<sup>238</sup>U]). Such maxima of <sup>210</sup>Pb<sub>xs</sub> and <sup>234</sup>Th<sub>t</sub> (Fig. 3) could have been produced as a consequence of the scavenging effects described above, and possibly, because Los Angeles' drinking or waste water contained, at that time, elevated levels of <sup>238</sup>U (Sweeney et al., 1980) and <sup>222</sup>Rn (Berelson and Hammond, 1987), which is the short-lived precursor of <sup>210</sup>Pb. In 1971, OC deposition rates were at their highest (Logan et al., 1989; Stull et al., 1996; Paulsen et al., 1999), and outfall sediments contributed close to 50% of the sediment input to the PV shelf (Santschi et al., 2000b). Because of this concentration control by the outfall, <sup>210</sup>Pb<sub>xs</sub> concentrations in surface sediments became a function of the OC concentrations and particle inputs (Paulsen et al., 1999).

The maximum concentration of measured <sup>234</sup>Th<sub>t</sub> ([<sup>234</sup>Th<sub>t</sub>] = [<sup>238</sup>U] + [<sup>234</sup>Th<sub>xs</sub>]) was confirmed as consisting of <sup>238</sup>U only by recounting samples after more than five half-lives (4 months), after which any <sup>234</sup>Th<sub>xs</sub>, if present, would have decayed away. High <sup>238</sup>U concentrations in Whites Point sewage sludge and PV surface sediments have been described for the early 1970s by Sweeney et al. (1980). These authors used uranium as one of their tracers for the dispersal of sewage-derived OC. <sup>238</sup>U (determined as total <sup>234</sup>Th) concentrations at depth significantly correlate with those of OC in the Palos Verdes sediments (Fig. 3), showing subsurface maxima at similar depths. Subsurface <sup>210</sup>Pb<sub>xs</sub> maxima had previously been described (Wheatcroft and Martin, 1994; Swift et al., 1996), but these authors did not adequately consider the cause for this <sup>210</sup>Pb anomaly.

Wheatcroft and Martin (1994) observed that this deep <sup>210</sup>Pb maximum only occurred in outfall affected sediments, and thus, recognized the anomalous nature of the <sup>210</sup>Pb profiles. Nonetheless, Swift et al. (1996) used it as a major piece of evidence to argue for deep bioturbation. However, their bioturbation model (Swift et al., 1996) fails to reproduce their <sup>210</sup>Pb<sub>xs</sub> profile when measured parameters are used.

### 3.2.2. Pre-1953 sedimentation rates

Suspended solids emission rates started to become significant in the 1950s (Young et al., 1975; Logan et al., 1989; Eganhouse and Venkatesan, 1993; Stull et al., 1996; Carry, 1996; Paulsen et al., 1999). Pre-1953 sediments, i.e., sediments below 65 cm depth in the vibra cores from sites 6C and 3C, were therefore less affected by the outfall sediments, and thus, because they experienced more constant conditions, can be used for sediment dating. According to the constant initial concentration (CIC) model, sedimentation rates can be calculated under steady state conditions and at relatively constant porosity, as follows:

$$[^{210}\text{Pb}_{\text{xs}}(z)] = [^{210}\text{Pb}_{\text{xs}}(0)] \exp(-\alpha z) \quad (3a)$$

$$\alpha = (\lambda/S) \quad (3b)$$

where [<sup>210</sup>Pb<sub>xs</sub>(z)] and [<sup>210</sup>Pb<sub>xs</sub>(0)] represent the excess <sup>210</sup>Pb concentration at depth z (cm) and at the sediment surface, respectively; λ = decay constant of <sup>210</sup>Pb (0.031 year<sup>-1</sup>); S = sedimentation rate in cm/year.

This approach furthermore assumes that particle reworking rates are negligible over the depth interval of the <sup>210</sup>Pb profile, and that fluxes of sediments and <sup>210</sup>Pb had been constant. In all Palos Verdes sediment cores we studied, sediment mixing depths averaged only about 2–3 cm (see Section 3.1). Therefore, the CIC model can be applied to <sup>210</sup>Pb<sub>xs</sub> data where sedimentation rates and <sup>210</sup>Pb fluxes varied little with time (likely a good approximation before 1953). Therefore, Eq. (3b) can directly yield estimates of sedimentation rates.

<sup>210</sup>Pb<sub>xs</sub> from pre-1953 sediments showed an exponential decrease, equivalent to a linear decrease in a semi-log plot (Fig. 9). This concentration decrease

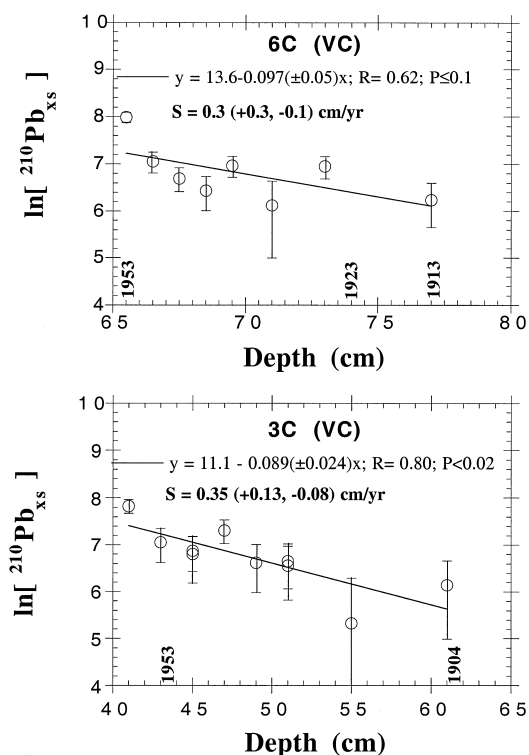


Fig. 9. Examples of  $^{210}\text{Pb}_{\text{xs}}$  ( $= [^{210}\text{Pb}(\text{total})] - [^{210}\text{Pb}(\text{supported})]$ ) profiles in vibra cores from sites 6C and 3C, shown as a semi-log plot for depths below the 1953 layer, where  $^{210}\text{Pb}_{\text{xs}}$  would have been little affected by scavenging of particles from the sewage outfall, and which does not contain any significant Pu and Cs nuclide activity (i.e., value  $\leq 3\sigma$  error). For 6C(VC), one elevated point at 74–76 cm was excluded from the correlation plot since this layer also showed elevated OC concentrations at the same depth. Sedimentation rates ( $S$ ) were calculated from the slope of  $\ln[^{210}\text{Pb}_{\text{xs}}(z)] = \ln[^{210}\text{Pb}_{\text{xs}}(0)] - (\lambda/S)z$ , with  $\lambda = \text{decay constant} = 0.03 \text{ year}^{-1}$ .

can be used to estimate a lower limit of the sedimentation rate. Because the outfalls started to operate in the late 1930s, these rates are lower limits because any particle flux enhancement effect would be highest near the top of such a pre-1953 profile. This would tend to steepen the best-fit line, i.e., increase the slope of the depth profile of  $^{210}\text{Pb}_{\text{xs}}$  in a semi-log plot, and thus make this sedimentation rate estimate a minimum. Had the particle and  $^{210}\text{Pb}$  flux been higher in the younger part of the profile, the true sedimentation rate would thus have been higher than 0.4 cm/year, the value we report here (Fig. 9). Non-linear curve-fitting to the data does not significantly change this value.

A sedimentation rate of 0.4 cm/year corresponds to a sediment accumulation rate of about  $0.5 \text{ g cm}^{-2}/\text{year}$  (Tables 1 and 2), which is significantly smaller than recent rates (obtained by Pu geochronology) of over  $0.8 \text{ g cm}^{-2}/\text{year}$ . The long-term sedimentation rates determined from different vibra (and box) cores vary little, and show better agreement than their errors suggest. The errors of the different estimates are such that the least-square fit lines are significant at the 90% (6C) or 98% (3C) confidence level (e.g., at 3C, Fig. 9,  $P < 0.02$ ). Normalization of  $^{210}\text{Pb}_{\text{xs}}$  to OC does not improve the confidence level of the least-square line, indicating that  $^{210}\text{Pb}_{\text{xs}}$  concentrations are not just a linear function of OC concentrations. These long-term sediment accumulation rates of about 0.4 to  $0.56 \text{ g cm}^{-2}/\text{year}$  agree well with geophysical measurements of Holocene sediment thickness of 20 m or higher (Lee, 1994), as they would have resulted in about 20–40 m of sediments in 6000–12,000 years, given a density of compacted sediments (below 1 m) of about  $1.5 \text{ g of dry sediment/cm}^3$  of wet sediment (our data, and Lee, 1994). They are also in agreement with rates determined by Paulsen et al. (1999) from numerically modeling  $^{210}\text{Pb}_{\text{xs}}$  and trace metal profiles taken from the early 1970s to the present time.

### 3.2.3. Comparison of sedimentation rates with literature values from the same sites

Our estimated sedimentation rates agree well with those of others determined for the same sites (Logan et al., 1989; Farley, 1990; Paulsen et al., 1999; Eganhouse and Kaplan, 1988; Eganhouse, 1996) (Table 2). However, our sedimentation rates challenge some previously held assumptions (Drake et al., 1994; Niedoroda et al., 1996) about the sedimentation regime on the PV shelf, and confirm the high end of previous estimates (Eganhouse and Kaplan, 1988; Logan et al., 1989; Farley, 1990; Drake et al., 1994; Wheatcroft and Martin, 1994; Lee, 1994; Niedoroda et al., 1996; Eganhouse, 1996; Swift et al., 1996; Paulsen et al., 1999; Eganhouse and Pontolillo, 2000). The reasons for any apparent discrepancies can be explained by one or several of the following reasons.

Many previous estimates were based on gravity cores (Eganhouse and Kaplan, 1988; Wheatcroft and Martin, 1994; Lee, 1994; Stull et al., 1996; Niedoroda

et al., 1996; Swift et al., 1996), which exhibited a documented but variable core top loss of 5–20 cm of surface sediment (Lee, 1994). Core top loss leads to variable and anomalously low estimates of recent sedimentation rates. Even when based on sub-cores taken from box cores, it is still possible to underestimate sedimentation rates (Santschi et al., 2000a). Some of the previous estimates interpreted  $^{210}\text{Pb}$  (Wheatcroft and Martin, 1994; Swift et al., 1996) as being a steady-state tracer, despite the fact that this nuclide is highly affected by boundary scavenging effects caused by the time-variable outfall derived particle emission rate on the PV shelf (Paulsen et al., 1999).

Some of the previous estimates relied on modeling of scarce data sets (Logan et al., 1989; Farley, 1990; Drake et al., 1994), and two assumptions: (a) the major source of the sediments was the outfall (Drake et al., 1994); (b) other sources such as the rivers and bluff and Portuguese Bend landslide toe erosion are minimal.

### 3.3. Sediment sources: evidence from radiocarbon measurements

What could be the source of the material transported across the shelf? There is good evidence that at shallower sites sediment reworking and resuspension is more frequent and intense, which can lead to subsequent re-deposition into the sediments at deeper stations ( $\geq 50$  m) (Lee, 1994). For example,  $\Sigma\text{DDT}$  and OC concentrations in sediments at sites shallower than about 40 m water depth are low and do not show any peaks (Lee, 1994), indicating intensive particle reworking and little accumulation of OC and contaminants. At water depths deeper than about 40–50 m, OC concentrations in sediment cores are substantially higher and peaks exist at 20–40 cm depth, depending on the time the core was taken and a possible surface sediment loss during coring (Lee, 1994). In addition, the sand content decreases, and silt and clay content increases perpendicular to and with distance from the shoreline (Drake, 1994). Episodic lateral transport events were recently demonstrated by Eganhouse (1994) for a site near 6C. High concentrations of certain compounds which were discharged into coastal waters predominantly

prior to the early 1970s, such as TAB and PCB compounds, were observed in 1993 in material collected by near bottom samplers attached to a Geoprobe (i.e., a benthic tripod for continuous boundary layer monitoring). Delayed deposition and other memory effects might thus be common features in Palos Verdes tracer profiles (Santschi et al., 2000b).

Due to higher wave energy dissipation rates at shallower depths, resuspension (scouring) rates are expected to be much higher near-shore, resulting in reduced fine sediment accumulation rates. Bioturbation in sediments at shallower water depth could allow fine-grained particles, which are enriched in OC, trace contaminants and radionuclides, to be buried and temporarily stored until sediment resuspension events “winnow” them out and redeposit them at greater water depths. This would lead to retardation of the offshore movement of these compounds. The sediment deposition rates at the 60 m line (3C, 5C, 6C, 8C) could thus be greatly affected by these scouring events at shallower sites. The record of off-shore movements of fine-grained sediments by these high-energy events would then be found in their profiles as layers of lower concentrations which interrupt layers of higher concentrations deposited in the 1950s to the 1970s (Fig. 4, and Santschi et al., 2000b). These sediment transport mechanisms can be further supported by our radiocarbon results.

Apparent radiocarbon ages of bulk sedimentary OC (SOC) are very old, up to 20,000 years, and even in the layers 4–6 cm and 58–60 cm below the surface of the less impacted sediments from site 3C, they are 3,100–5,800 years, and vary non-systematically from 2–4 ky at site 6C (Table 3). In addition, foraminifera from site 3C, below the effluent-affected zone, have an apparent  $^{14}\text{C}$  age of 5000–11,000 years (Table 4). Even in layers that were deposited in the mid-1800s (91 cm in core 3C(VC) estimated by  $^{210}\text{Pb}_{\text{xs}}$  as having been deposited in the mid-1800s), the apparent  $^{14}\text{C}$  age of these forams is still 9800 years. Also, even though apparent  $^{14}\text{C}$  ages of forams at 6C are younger, their youngest apparent age occurs at the bottom of the core, at 137 cm. All forams show strong signs of corrosion, especially in sediment layers shallower than 120 cm, which were likely deposited in the early 1800s or later. The fact that apparent radiocarbon ages are 3000 and 5000

Table 3  
Radiocarbon results<sup>a</sup> of bulk OC and foraminifera from sediment cores 3C(VC) and 6C(VC)

Depth interval (cm)	% OC	Apparent age (year) of OC ( $\pm 1\sigma$ )	Fraction modern of OC ( $\pm 1\sigma$ )	$\delta^{13}\text{C}$ (‰) of OC	Apparent age (year) of forams ( $\pm 1\sigma$ )	Fraction modern of forams ( $\pm 1\sigma$ )	$\delta^{13}\text{C}$ (‰) of forams
<i>3C(VC)</i>							
4–6	2.4	3130 $\pm$ 40	0.68 $\pm$ 0.0033	–22.32	1420 $\pm$ 55 <sub>b</sub>	0.8381 $\pm$ 0.0057 <sub>b</sub>	0.00 <sub>b</sub>
58–60	–	5770 $\pm$ 45	0.49 $\pm$ 0.0027	–22.11	–	–	–
90–92	–	7060 $\pm$ 35	0.415 $\pm$ 0.0019	–21.77	9830 $\pm$ 120	0.2943 $\pm$ 0.0043	–0.47
120–122	–	9950 $\pm$ 45	0.29 $\pm$ 0.0016	–22.22	7670 $\pm$ 140	0.3848 $\pm$ 0.0069	–0.18
130–132	–	–	–	–	5270 $\pm$ 130	0.5192 $\pm$ 0.0084	0.19
150–152	–	12,150 $\pm$ 50	0.22 $\pm$ 0.0013	–21.90	10,500 $\pm$ 80	0.2700 $\pm$ 0.0027	–0.98
160–162	–	19,750 $\pm$ 140	0.086 $\pm$ 0.0015	–22.56	10,850 $\pm$ 90	0.2587 $\pm$ 0.0029	–0.55
160–162	–	–	–	–	10,650 $\pm$ 75	0.2648 $\pm$ 0.0025	–0.78
<i>6C(VC)</i>							
0–1	2.05	2770 $\pm$ 35	0.708 $\pm$ 0.003	–	–	–	–
28–29	6.55	2150 $\pm$ 30	0.765 $\pm$ 0.003	–	–	–	–
43–44	3.09	2080 $\pm$ 30	0.772 $\pm$ 0.003	–	–	–	–
66–67	0.77	3400 $\pm$ 30	0.655 $\pm$ 0.003	–	–	–	–
72–74	1.1	3170 $\pm$ 50	0.674 $\pm$ 0.004	–	–	–	–
98–100	0.44	3640 $\pm$ 45	0.635 $\pm$ 0.003	–	1950 $\pm$ 85	0.7844 $\pm$ 0.0083	0.32
118–120	0.43	–	–	–	1910 $\pm$ 85	0.7879 $\pm$ 0.0082	–0.05
136–138	0.42	3960 $\pm$ 30	0.611 $\pm$ 0.003	–	1450 $\pm$ 95	0.8353 $\pm$ 0.0097	–0.09

<sup>a</sup><sup>14</sup>C:  $t_{1/2}$  = 5568 year was used for age calculation; fraction modern is generally defined as the atom concentration related to 0‰ = prebomb (1950); <sup>14</sup>C values were corrected for fractionation using measured  $\delta^{13}\text{C}$  values, or to –22.0‰ when none were available.  $1\sigma$  = 1 standard deviation.

<sup>b</sup>The apparent age, fraction modern, and  $\delta^{13}\text{C}$  values given for the 58–60 cm depth of core 3C(VC) are the same as those for the 4–6 cm sample, as these values were derived from a 0–60-cm composite. This large depth interval was required due to the low abundance of forams in these surface sediments.

Table 4

Sediment inventories (in dpm cm<sup>-2</sup> for radionuclides, and mg cm<sup>-2</sup> for OC) in the post-1953 layers

Site (core)	<sup>239,240</sup> Pu	<sup>137</sup> Cs	<sup>210</sup> Pb <sub>xs</sub>	<sup>234</sup> Th <sub>xs</sub>	OC
8C	–	9	224	–	1491
6C	2.60	10.8	272	8.7, 5.0, 4.0 <sup>a</sup>	1409, 1286, 1225, 909 <sup>a</sup>
6C(VC)	3.45	13.7	317	–	1557
5C	1.71	14.3	388	15.3	1505
3C	0.98	8.4	305	10.3	1500
3C(VC)	1.09	12.6	312	20.7	–
Expected inventory	0.25 <sup>b</sup>	10 <sup>b</sup>	7 <sup>c</sup>	14 <sup>d</sup>	–

<sup>a</sup>Results from determinations in multiple cores.

<sup>b</sup>Wong et al. (1992).

<sup>c</sup>Fuller and Hammond (1985).

<sup>d</sup>Based on <sup>238</sup>U of 2.4 dpm/l and 60 m water depth.

years in sediments deposited within the last 100 years, based on <sup>210</sup>Pb dating, therefore strongly suggests that radiocarbon values of bulk SOC contain a variety of components with different apparent <sup>14</sup>C ages (Guo et al., 1996; Guo and Santschi, 2000). Therefore, <sup>14</sup>C ages cannot be used in a simple way for sediment dating of Palos Verdes shelf sediments.

Alternative approaches of data normalization to surface values (Jones, 1994) are of no help here either. While the apparent <sup>14</sup>C ages of organic carbon at depths that were minimally affected by the outfall would suggest a long-term sediment accumulation rate of 0.1 cm/year (Fig. 10a), that rate would also have to apply over the upper 70 cm, where it is > 1 cm/year, more than 10 times higher, which obviously leads to serious inconsistencies in interpretations. At site 3C, one would be left with apparent <sup>14</sup>C ages of over 17,000 years at depths of 151–161 cm, a layer that should only be about 250 years old, according to extrapolations from <sup>210</sup>Pb dating. Furthermore, sediments at 58–60 cm depth from this site, which are only about 90 years old, and thus contain significant <sup>210</sup>Pb<sub>xs</sub> activities, would still have an apparent <sup>14</sup>C age of about 2700 years. Correlation between  $\delta^{13}\text{C}$  and apparent <sup>14</sup>C age of forams (Fig. 10b) indicates that the older the forams, the lower their  $\delta^{13}\text{C}$  values, which is in agreement with the relationship seen in other parts of the world's ocean.

In summary, <sup>14</sup>C ages and sedimentation rates derived from these apparent ages are not reliable for

the Palos Verdes shelf, and suggest that SOC and forams deposited at 60 m water depth mostly originate from previously stored material at shallower depths, and/or from other sources to the area with a variable age. This must be true for these sediments even before the existence of the outfall.

These old <sup>14</sup>C ages, therefore, support a conceptual model, which states that a significant fraction of organic matter deposited in these sediments before the outfall, as well as now, is generally refractory and supplied from secondary sources. Sources other than wastewater include winnowed silt from shallower sediments, bluff and Portuguese Bend landslide toe erosion, and terrestrial organic matter from river washloads. All of these sediment sources likely contain significant fractions of old OC. Relatively

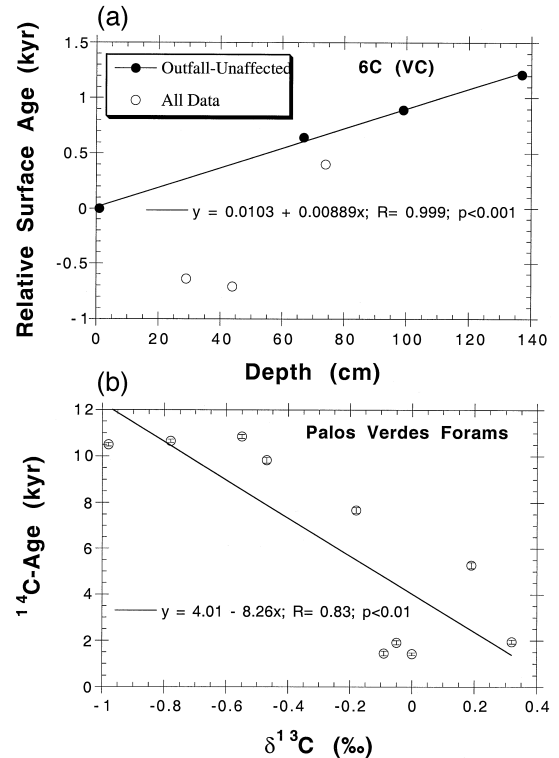


Fig. 10. (a) <sup>14</sup>C surface age relative to the sediment surface (Jones, 1994) as a function of depth at site 6C. (b) Correlation between  $\delta^{13}\text{C}$  and apparent <sup>14</sup>C age of forams. The sedimentation rate, *S*, between 0 and 70 cm could be calculated from these data as 0.11 cm/year; however, *S* is larger than 1 cm/year in this region, based on the thickness of the effluent affected layer and the known beginning of effluent discharge.

old OC being swept off the PV shelf has been observed before in suspended sediments by Emery (1960) and Williams et al. (1992). Furthermore, Sweeney et al. (1980) reported depleted  $\delta^{13}\text{C}$  values for the OC enriched sediments characteristic of terrestrial OC.

The heterogeneity of foraminifera (in terms of species composition, degree of corrosion, and shapes) in these sediments further supports the dynamic and episodic deposition and the influence of cross-shelf transport processes in this shelf area. Additional sources of old ( $\Delta^{14}\text{C} \ll 0\%$ ) OC might include hydrocarbons from natural seeps (Eganhouse and Venkatesan, 1993), oil and grease from the outfall (Eganhouse and Venkatesan, 1993; Eganhouse, 1978), and soot carbon (Gustafsson and Gschwend, 1998). However, soot carbon only makes up 3–4% of the OC at site 6C (Gustafsson and Gschwend, 1998). Even though oil, grease and hydrocarbons can constitute a significant percentage of the total OC in the outfall-affected sediments ( $\leq 40\%$  of the OC in sediments deposited in 1976–1977, Eganhouse and Venkatesan, 1993; Eganhouse, 1978), pre-outfall sediments resemble the sediments from other non-impacted sites nearby, which have total hydrocarbon concentrations of the order of a few per mil of the OC concentration. This suggests that old, refractory OC from terrestrial and sedimentary sources and corrosion resistant foraminifera are stored in inner-shelf sediments up to 10,000 years before they are transported further offshore, likely related to storm events.

Sediment inventories of selected radionuclides and OC, summarized in Table 4, lend further support to the suggested transport mechanisms. Both short-lived but particle-reactive tracers, such as  $^{234}\text{Th}$ , and more soluble bomb test fallout nuclides, such as  $^{137}\text{Cs}$ , are found in the sediments in amounts that are close to the levels expected from their production or fallout rates. However, longer-lived and particle-reactive tracers, such as  $^{239,240}\text{Pu}$  and  $^{210}\text{Pb}$ , are found in these sediments in much greater amounts than expected from their deposition rates into the water column (Table 4). For example, the inventory of the bomb-fallout nuclide  $^{239,240}\text{Pu}$  is enhanced by a factor of 5–10, while the inventory of  $^{210}\text{Pb}$  in these sediments is greater than that expected from local atmospheric delivery by a factor of 20–50. This can

only be explained by a “boundary scavenging” effect, whereby particle-reactive nuclides are scavenged out of large volumes of seawater by localized regions of higher particle fluxes, a process which is aided by the large dilution demand of the outfall water (Paulsen et al., 1999). Changes in particle dynamics would thus give rise to highly concentrated regions in underlying sediments during times of high particle flux and depleted regions elsewhere where the particle flux is lower. Since such enhancements require larger space and time scales, they are mainly seen for longer-lived nuclides under steady-state situations (such as  $^{210}\text{Pb}$ ), but not for short-lived  $^{234}\text{Th}$ .

The difference between the inventories of  $^{210}\text{Pb}$  and  $^{239,240}\text{Pu}$ , both particle-reactive nuclides, can be explained as follows: The greater enhancement of  $^{210}\text{Pb}$  over that of  $^{239,240}\text{Pu}$  is likely due to the different delivery mechanisms from the atmosphere (Santschi and Honeyman, 1989). Because  $^{210}\text{Pb}$  is delivered continuously, every year, from the atmosphere, and is also supplied from upwelled waters,  $^{210}\text{Pb}$  fluxes to the sediments can be enhanced continuously. On the other hand, concentrations of  $^{239,240}\text{Pu}$ , which was delivered more like a pulse input with a maximum in 1963, are depleted in surface waters. Pu has been found since the 1970s mostly in a subsurface peak centered around 400 m water depth (Wong et al., 1992), which is well out of contact with the water at 60 m depth. Thus, differences in source functions between  $^{210}\text{Pb}$  and  $^{239,240}\text{Pu}$  resulted in different enhancements in sediments (Table 4).

### 3.4. Sediment transport on the Palos Verdes shelf

One of the most striking features of many tracer concentration profiles is the multiple peaks profile in the high concentration region (Fig. 4). All profiles of radionuclides (e.g.,  $^{137}\text{Cs}$ ,  $^{239,240}\text{Pu}$ ,  $^{210}\text{Pb}$  and  $^{234}\text{Th}$ , given in Appendix A (Tables A1–3), with examples given in Fig. 4), OC, and porosity (Fig. 7b), but not of grain size distribution (given in Fig. 7c) exhibit multiple peaks at sites 6C and 8C (close to outfall), but not at 3C (farther away from outfall, Fig. 5). Many, but not all trace metal profiles in cores collected in the 1980s by LACSD (unpublished data, partly shown in Santschi et al., 2000b, and List and

Paulsen, 2000) and some of the DDE profiles measured in the 1990s by USGS (Lee, 1994) show such features as well. The likely reason that these multiple peak features have not often been reported in the literature is that cross-shelf transport events, which might have led to the small-scale spatial variability we observe now, are of episodic nature. Episodic sediment transport events, which have been described in the literature, include storm-related coastal erosion and river washloads (Inman and Jenkins, 1999), with major storm events of the past 35 years in 1969, 1978, 1980, 1983, 1993, and 1995. The 1969 storm could have been responsible for splitting some OC and radionuclide peaks into two major peaks.

According to Drake (1994) and Drake et al. (1994), the major sources of sediments to the PV shelf come from (1) riverine inputs, especially during flooding events; (2) erosion of shore line, bluff and Portuguese Bend landslide toe sediments; and (3) White's Pt. waste water outfalls, which peaked in 1971. Our grain size distributions (e.g., Fig. 7c), however, cannot distinguish between these different sources since all sources of sediments reaching off-shore areas (> 40 m water depth) are considered as fine-grained (Drake et al., 1994; Lee, 1994).

It can be calculated that only in the late 1960s and early 1970s were particles from the White's Pt. Waste water outfalls a significant fraction of Palos Verdes deposits (Santschi et al., 2000b). However, since that time, the direct contribution of the White's Pt. outfalls to the sedimentary deposits on the Palos Verdes shelf must have decreased greatly since the sediment load from the outfall has declined by about an order of magnitude (Farley et al., 1990; Eganhouse and Venkatesan, 1993; Drake, 1994; Stull et al., 1996; Carry, 1996; Paulsen et al., 1999). Other sources must have remained active, or in some cases have increased. For example, since the flow of nutrient enriched water from the treatment plant had remained relatively constant (or increased slightly) from 1971 to the present (Farley et al., 1990; Stull et al., 1996; Carry, 1996), coastal productivity and thus, locally enhanced organic sedimentation through flocculation effects during and after plume rise (Logan et al., 1989; Farley, 1990) likely remained constant. Sediment inputs from palisades and landslide erosion is still continuing as well. Large

amounts of sediment were deposited on the PV shelf, especially at site 3C from the movement of a local landslide (Portuguese Bend Landslide) since the 1980s (Drake et al., 1994; Kayen et al., 1994). Sediment from the toe of the landslide was redistributed by several large storms that took place in this region, e.g., during 1982/1983 and 1988 (Kayen et al., 1994), causing episodic deposition recorded in the sediments. Landslide sources are also supported by the observation that mineral compositions of surface sediments collected near station 3C in 1992 contain sediment tracers characteristic of Portuguese Bend composition (e.g., augite with high Ti content), as described in Wong (1994).

Most importantly, riverine inputs to the coastal region during pulsed discharge events (Gorsline, 1992; Inman and Jenkins, 1999), are extraordinarily high, despite engineering alterations in recent times. Most riverine sediment supplied during winter storm and flood events is transported to the depositional areas on the shelf through cross-shelf exchange in benthic nepheloid layers (Karl, 1976, 1994; Drake et al., 1985). For example, fully developed benthic nepheloid layers with high turbidity levels were observed near the bottom at site 6C (Wheatcroft and Martin, 1994), even under excellent weather conditions (i.e., minimal swell). The heavy mineral fraction of the sediments on the Palos Verdes shelf is rich in hornblende (Wong, 1994), a mineral that originates from regional rivers. In addition, particles from river flooding can be moved offshore as turbid plumes as far as 60–100 km from the shoreline during coastal upwelling events initiated during such river floods, as is evident from satellite-derived images (Hickey and Kachel, 2000).

Such a conceptual model incorporating these processes is also in agreement with the view of Eganhouse and Venkatesan (1993), who emphasized that the emission of suspended silts and total OC in contemporary surface runoff (Schwalbach and Gorsline, 1985) is significantly higher than present-day suspended solids discharge rates from municipal wastewater outfalls. Furthermore, Kayen et al. (1994) argued that shore-line and Portuguese Bend landslide toe erosion are still important and make major contributions to the sediment budget of this region, in support of our estimates of relatively high values of recent sediment accumulation rates.

Zeng and Venkatesan (1999) and Zeng et al. (1999) recently concluded from water column measurements that significant quantities of pollutants such as DDT compounds are lost from Palos Verdes shelf sediments by resuspension and transport over large distances. This conclusion was, however, based on assuming that degradation of DDTs, rapid particle settling and riverine sources of these pollutants can be ignored. These assumptions are erroneous, as (1) biodegradation of DDTs occurs (Quensen et al., 1999), even at 10–12°C bottom water temperatures, (2) riverine sources of particles and particle-associated

pollutants to the site are large (e.g., Inman and Jenkins, 1999; Inman et al., 2000; Hickey and Kachel, 2000), (3) the standing stock of resuspended particles in a benthic nepheloid layer is mainly lost by particle settling to the underlying sediments rather than by export, with typical turnover times for nepheloid particles of hours rather than days (Santschi et al., 1983; Bacon and Van der Loeff, 1989; Baskaran et al., 1996), and (4) particle and pollutant deposition on the Palos Verdes shelf is currently the dominant process (see previous discussion). Therefore, there is little evidence to suggest that particle and particle-associated

Table A1

<sup>234</sup>Th data (1 SD = 1 standard deviation; supported <sup>234</sup>Th activity (<sup>234</sup>Th<sub>supp</sub>) is the average over several depth intervals)

6C(BC1)			6C(BC3)			6C(BC4)		
Depth (cm)	<sup>234</sup> Th <sub>xs</sub> (dpm/kg)	± 1 SD	Depth (cm)	<sup>234</sup> Th <sub>xs</sub> (dpm/kg)	± 1 SD	Depth (cm)	<sup>234</sup> Th <sub>xs</sub> (dpm/kg)	± 1 SD
0–1	6053	866	0–1	6874	1760	0–1	7512	854
1–2	2474	796	1–2	5314	1835	1–2	3887	785
2–3	–207	841	2–3	1279	1836	2–3	2619	807
3–4	336	810	3–4	3070	1878	3–4	867	999
4–5	1181	800	4–5	–280	1719	3–4	3808	850
6–7	–206	943	5–6	3111	2141	4–5	392	830
9–10	383	949	6–7	–147	2133	5–6	1566	838
						6–7	700	922
	( <sup>234</sup> Th <sub>supp</sub> = 2400 ± 400)			( <sup>234</sup> Th <sub>supp</sub> = 2400 ± 400)			( <sup>234</sup> Th <sub>supp</sub> = 2500 ± 400 at 0–9 cm) ( <sup>234</sup> Th <sub>supp</sub> = 4200 ± 500 at 10–12 cm)	
3C(BC)			3C(VC)			5C(BC)		
Depth (cm)	<sup>234</sup> Th <sub>xs</sub> (dpm/kg)	± 1 SD	Depth (cm)	<sup>234</sup> Th <sub>xs</sub> (dpm/kg)	± 1 SD	Depth (cm)	<sup>234</sup> Th <sub>xs</sub> (dpm/kg)	± 1 SD
0–1	8161	1131	0–1	7980	1100	0–1	8878	852
1–2	3794	1171	2–3	2830	1000	1–2	5411	1101
2–3	1605	1209	4–5	–1500	2500	1–2	6028	2742
3–4	834	1173	6–7	1940	650	1–2	82	3232
4–5	182	1329	6–7	630	1290	2–3	3198	1209
5–6	–271	1195				2–3	443	2456
						3–4	2274	1131
						3–4	–2884	3458
						4–5	858	792
						5–6	2037	1172
						5–6	4102	3523
						6–7	977	2017
	( <sup>234</sup> Th <sub>supp</sub> = 2150 ± 400)			( <sup>234</sup> Th <sub>supp</sub> = 2700 ± 400)			( <sup>234</sup> Th <sub>supp</sub> = 2700 ± 400)	

Table A2

<sup>210</sup>Pb data (1 SD = 1 standard deviation; dup = duplicate)

Depth (cm)	3C-VC3-A <sup>210</sup> Pb-α total		<sup>210</sup> Pb-α excess	
	(dpm/kg)	± 1 SD	(dpm/kg)	± 1 SD
	0–1	12,477	934	10,277
6–7	9559	807	7359	810
10–11	8558	396	6358	402
14–15	7931	536	5731	540
20–21	9691	363	7491	370
30–31	11,216	483	9016	488
34–35	10,029	579	7829	583
36–37	7531	338	5331	345
40–41	4708	197	2508	209
42–43	3357	273	1157	282
42–43	3982	259	1782	268
44–45	3099	185	899	198
44–45(#2)	3163	155	963	170
46–47	3694	220	1494	231
48–49	2949	192	749	204
50–51	2902	206	702	217
50–51(#2)	2972	170	772	184
52–53	2247	98	–	–
54–55	2090	136	–	–
54–55(#2)	2146	104	–	–
54–55(#3)	2205	162	–	–
56–57	1946	84	–	–
58–59	2575	137	–	–
60–61	2664	102	–	–
60–61(#2)	2437	142	–	–
65–66	2060	127	–	–
70–71	1771	147	–	–
80–81	2143	108	–	–
100–101	1852	168	–	–
120–121	2259	138	–	–
120–141	2523	217	–	–
161–161	2385	213	–	–
Depth (cm)	5C-BC1-C <sup>210</sup> Pb-α total		<sup>210</sup> Pb-α excess	
	(dpm/kg)	± 1 SD	(dpm/kg)	± 1 SD
	0–1	10,606	668	8606
4–5	11,154	510	9154	520
9–10	12,525	457	10,525	468
14–15	10,265	455	8266	466
19–20	6083	307	4084	323
19–20(dup)	10,854	543	8854	552
24–25	9495	483	7495	493
29–30	11,825	650	9825	657
29–30(dup)	13,732	677	11,732	685
34–35	11,484	630	9485	638
39–40	12,885	653	10,885	660
39–40(dup)	12,874	636	10,874	644
44–45	11,378	700	9378	707

Table A2 (continued)

Depth (cm)	5C-BC1-C <sup>210</sup> Pb-α total		<sup>210</sup> Pb-α excess	
	(dpm/kg)	± 1 SD	(dpm/kg)	± 1 SD
	44–45(dup)	11,645	464	9645
49–50	10,564	620	8564	628
49–50(dup)	11,822	792	9822	798
54–55	9239	551	7239	560
56–57	9204	297	7204	313
58–59	9248	702	7248	709
59–60	6360	250	4361	269
62–63	4577	323	2577	339
64–65	3523	227	1523	248
Depth (cm)	6C-VC <sup>210</sup> Pb-α total		<sup>210</sup> Pb-α excess	
	(dpm/kg)	± 1 SD	(dpm/kg)	± 1 SD
	0–2	12,263	387	10,363
10–11	11,834	499	9934	502
18–19	11,984	275	10,084	281
21–22	13,651	390	11,751	395
25–26	15,022	463	13,122	467
25–26	14,367	498	12,467	501
29–30	13,558	345	11,658	350
31–32	10,572	296	8672	302
33–34	10,089	410	8189	414
35–36	10,967	344	9067	349
39–40	10,423	205	8523	214
44–45	9366	244	7466	252
47–48	10,960	408	9060	412
50–51	10,635	340	8735	345
53–54	9823	372	7923	376
54–55	8186	297	6286	303
54–55	8504	317	6604	322
56–57	9532	387	7632	392
57–58	9128	408	7228	412
60–61	8592	339	6692	344
62–63	8526	270	6626	276
63–64	8399	531	6499	535
64–65	7718	371	5818	376
64–66	7781	396	5881	400
65–66	4851	262	2951	269
66–67	3059	195	1159	204
67–68	2710	120	810	134
68–69	2523	146	623	158
69–70	2958	160	1058	171
70–72	2355	262	455	269
72–74	2942	180	1042	190
74–76	3894	214	1994	223
76–78	2410	159	510	170
78–80	1933	95	–	–
82–84	2156	149	–	–
84–86	1818	120	–	–
88–90	1810	92	–	–

Table A2 (continued)

Depth (cm)	6C-VC		<sup>210</sup> Pb-α total		<sup>210</sup> Pb-α excess	
	<sup>210</sup> Pb-γ total					
	(dpm/kg)	± 1 SD	(dpm/kg)	± 1 SD	(dpm/kg)	± 1 SD
90–92	2119	136	–	–	–	–
92–94	2018	92	–	–	–	–
104–106	1607	65	–	–	–	–
114–116	1905	118	–	–	–	–
126–128	2043	130	–	–	–	–
136–138	1732	121	–	–	–	–
Depth (cm)	8C-BC1		<sup>210</sup> Pb-γ total		<sup>210</sup> Pb-α excess	
	<sup>210</sup> Pb-γ total					
	(dpm/kg)	± 1 SD	(dpm/kg)	± 1 SD	(dpm/kg)	± 1 SD
0–1	10,927	572	9027	580	–	–
9–10	10,721	530	8821	539	–	–
15–16	11,176	656	9276	664	–	–
19–20	11,713	299	9813	315	–	–
24–25	10,535	574	8635	582	–	–
27–28	8601	562	6701	571	–	–
29–30	10,026	478	8126	488	–	–
29–30	10,187	668	8287	676	–	–
31–32	8883	697	6983	704	–	–
31–32	8891	602	6991	610	–	–
34–35	6562	656	4662	664	–	–
39–40	7846	432	5946	443	–	–
44–45	6967	690	5067	698	–	–
49–50	7482	538	5582	548	–	–
52–53	3750	524	1850	534	–	–

sociated pollutant export by erosion from the contaminated Palos Verdes site is currently a major process.

#### 4. Summary and conclusions

Given the abundance of sediment sources to the Palos Verdes shelf, the episodic nature of some of these sources, the fine-grained nature of the accumulating sediments at the 60 m sites, the high sedimentation rates and shallowness of the particle mixed layers, contaminants presently buried 30–50 cm deep should continue to move deeper into the sediments where they are less available for bioaccumulation and food chain transfer. This is consistent with the observation that surface concentrations of contaminants such as DDTs remained elevated and relatively constant over the past 10–15 years (Lee, 1994, and LACSD, unpublished data) and that these com-

Table A3  
<sup>137</sup>Cs and <sup>239,240</sup>Pu data (1 SD = 1 standard deviation)

Depth (cm)	Porosity	<sup>137</sup> Cs		<sup>239,240</sup> Pu	
		(dpm/kg)	± 1 SD	(dpm/kg)	± 1 SD
<i>3C-BC1-A</i>					
0–1	0.70	172	30	15	2
1–2	0.70	220	41	–	–
1–2(#2)	0.70	214	32	–	–
2–3	0.67	172	37	–	–
3–4	0.65	287	41	13	1
3–4(#2)	0.65	124	37	–	–
4–5	0.64	172	40	–	–
5–6	0.63	214	39	–	–
5–6(#2)	0.63	163	30	–	–
6–7	0.61	151	36	–	–
7–8	0.59	191	36	–	–
7–8(#2)	0.59	107	33	–	–
8–9	0.59	176	34	–	–
9–10	0.59	236	37	18	2
14–15	0.59	145	33	20	2
19–20	0.61	179	39	19	2
19–20(#2)	0.61	158	40	18	2
24–25	0.61	165	39	22	2
24–25(#2)	0.61	122	29	–	–
27–28	0.66	277	38	36	3
29–30	0.64	353	45	45	4
30–31	0.65	283	44	–	–
31–32	0.65	265	40	52	5
34–35	0.56	167	40	25	3
39–40	0.56	184	34	16	1
43–44	0.52	73	25	9	1
44–45	0.50	59	29	5	1
48–49	0.49	106	26	11	1
48–49				10	1
<i>3C-VC3-A</i>					
0–1	0.68	226	28	17	2
2–3	0.66	287	39	–	–
2–3(#2)	0.66	185	35	–	–
4–5	0.68	185	37	–	–
4–5(#2)	0.68	163	39	–	–
6–7	0.66	322	52	–	–
6–7(#2)	0.66	241	46	–	–
6–7(#3)	0.66	199	32	–	–
8–9	0.62	89	34	18	2
10–11	0.60	159	39	–	–
10–11(#2)	0.60	193	29	–	–
14–15	0.60	160	40	–	–
20–21	0.64	185	35	19	2
20–21	0.64	204	35	21	2
24–25	0.61	210	42	19	2
26–27	0.63	179	37	24	2
28–29	0.65	249	38	–	–
30–31	0.67	404	57	51	4
30–31	0.67	327	37	44	3

(continued on next page)

Table A3 (continued)

Depth (cm)	Porosity	<sup>137</sup> Cs		<sup>239,240</sup> Pu	
		(dpm/kg)	± 1 SD	(dpm/kg)	± 1 SD
<i>3C-VC3-A</i>					
32–33	0.67	297	40	55	5
34–35	0.67	284	43	62	5
36–37	0.63	189	34	–	–
40–41	0.54	108	33	11	1
44–45	0.53	148	33	–	–
50–51	0.50	66	29	5	1
50–51(dup)	0.50	–	–	5	1
50–51(#2)	0.50	54	25	–	–
52–53	0.50	32	27	–	–
54–55	0.48	36	22	–	–
54–55(#2)	0.48	56	32	–	–
59	0.51	0	0	–	–
61	0.52	106	34	3	1
61(#2)	0.52	60	30	–	–
66	0.50	55	22	–	–
66(#2)	0.50	58	22	–	–
71	0.50	37	29	1	0
76	0.47	39	32	–	–
76(#2)	0.47	20	26	–	–
81	0.48	54	26	1	0
86	0.48	16	28	0	0
86(#2)	0.48	48	25	–	–
91	0.49	107	31	0	0
91(#2)	0.49	32	24	0	0
101	0.49	32	23	0	0
111	0.47	13	19	–	–
116	0.46	74	29	–	–
121	0.46	57	33	0	0
126	0.47	44	24	–	–
131	0.48	45	21	–	–
136	0.48	18	20	–	–
141	0.50	26	19	0	0
146	0.49	46	21	–	–
151	0.47	30	19	–	–
<i>5C-BC1-C</i>					
0–1	0.71	310	46	17	2
1–2	0.70	148	39	–	–
1–2(#2)	0.70	262	45	–	–
1–2(#3)	0.70	172	39	–	–
2–3	0.70	274	45	–	–
2–3(#2)	0.70	143	37	–	–
3–4	0.70	176	39	–	–
3–4(#2)	0.70	228	41	–	–
4–5	0.70	223	42	22	2
5–6	0.70	232	44	–	–
5–6(#2)	0.70	134	40	–	–
6–7	0.69	188	46	–	–
7–8	0.69	196	44	–	–
7–8(#2)	0.69	200	40	–	–
8–9	0.69	286	47	–	–
9–10	0.69	240	40	19	2

Table A3 (continued)

Depth (cm)	Porosity	<sup>137</sup> Cs		<sup>239,240</sup> Pu	
		(dpm/kg)	± 1 SD	(dpm/kg)	± 1 SD
<i>5C-BC1-C</i>					
14–15	0.67	252	35	26	3
19–20	0.67	330	43	21	2
22–23	0.67	234	46	20	3
24–25	0.67	268	48	24	2
29–30	0.71	299	48	35	3
34–35	0.75	535	54	67	5
36–37	0.77	571	53	–	–
38–39	0.77	532	50	–	–
39–40	0.75	466	54	73	7
40–41	0.73	421	60	–	–
42–43	0.75	467	51	71	5
44–45	0.77	559	57	97	7
47–48	0.77	426	47	68	5
49–50	0.77	370	57	113	16
50–51	0.77	363	63	68	5
52–53	0.76	260	56	48	4
54–55	0.74	284	47	34	3
58–59	0.68	211	35	28	2
59–60	0.64	193	40	18	2
59–60(dup)	–	–	–	17	2
62–63	0.53	105	30	4	1
64–65	0.51	112	23	4	1
<i>6C-VC</i>					
0–2	0.69	259	44	34	2
2–3	0.72	212	45	–	–
3–4	0.73	287	43	–	–
4–5	0.73	187	46	–	–
9–10	0.69	202	35	42	3
14–15	0.72	333	44	–	–
17–18	0.74	–	–	71	4
19–20	0.75	436	42	–	–
21–22	0.78	–	–	109	7
24–25	0.78	492	54	129	8
26–27	0.78	–	–	135	11
29–30	0.80	563	60	–	–
30–31	0.77	–	–	98	5
32–33	0.77	321	49	–	–
32–33	0.77	308	52	–	–
34–35	0.79	442	49	130	9
36–37	0.78	–	–	100	7
37–38	0.75	332	50	85	8
38–39	0.80	–	–	164	10
39–40	0.80	505	58	–	–
42–43	0.74	248	42	79	5
44–45	0.70	283	35	73	4
46–47	0.73	–	–	82	4
49–50	0.76	247	44	113	5
52–53	0.77	–	–	126	8
54–55	0.75	223	39	–	–
55–56	0.76	–	–	91	6
57–58	0.75	–	–	73	5

Table A3 (continued)

Depth (cm)	Porosity	<sup>137</sup> Cs		<sup>239,240</sup> Pu	
		± 1 SD		± 1 SD	
		(dpm/kg)		(dpm/kg)	
<i>6C-VC</i>					
59–60	0.76	223	39	–	–
60–61	0.74	–	–	69	5
64–65	0.73	239	33	28	2
66–67	0.55	–	–	0	2
69–70	0.53	54	26	1	2
69–70	0.53	–	–	2	2
72–74	0.53	–	–	3	2
80–82	0.52	< 30	–	5	3
80–82	0.52	–	–	5	3
90–92	0.50	53	23	–2	2
90–92	0.50	35	30	–	–
100–102	0.48	78	27	–	–
100–102	0.48	42	18	–	–
110–112	0.48	< 30	–	–	–
<i>6C-BC4</i>					
0–1	0.71	195	32	18	2
1–2	0.69	109	36	–	–
1–2	0.69	202	39	–	–
2–3	0.68	204	32	–	–
2–3	0.68	187	40	–	–
2–3	0.68	186	35	–	–
3–4	0.70	246	37	–	–
4–5	0.69	168	40	25	3
5–6	0.69	160	40	–	–
6–7	0.68	145	33	–	–
9–10	0.70	277	41	–	–
10–11	0.67	–	–	27	2
10–11	0.67	–	–	43	4
11–12	0.69	282	43	–	–
14–15	0.70	278	41	47	3
19–20	0.71	–	–	50	5
21–22	0.74	362	45	–	–
24–25	0.74	–	–	83	5
27–28	0.77	–	–	131	8
29–30	0.75	316	36	94	5
31–32	0.79	–	–	137	9
32–33	0.78	–	–	119	8
33–34	0.77	481	55	143	9
34–35	0.76	480	43	106	6
36–37	0.76	–	–	103	8
37–38	0.76	345	46	–	–
38–39	0.76	–	–	144	8
38–39	0.76	–	–	135	7
39–40	0.75	323	45	108	7
40–41	0.76	–	–	93	7
42–43	0.77	231	40	112	9
44–45	0.79	334	34	126	10
45–46	0.77	–	–	96	8
47–48	0.77	331	43	76	5
49–50	0.74	156	42	57	5
52–53	0.75	205	41	56	5

Table A3 (continued)

Depth (cm)	Porosity	<sup>137</sup> Cs		<sup>239,240</sup> Pu	
		± 1 SD		± 1 SD	
		(dpm/kg)		(dpm/kg)	
<i>6C-BC4</i>					
54–55	0.70	116	33	–	–
55–56	0.69	178	34	14	2
<i>8C-BC1</i>					
0–1	0.70	124	33	–	–
9–10	0.70	133	32	–	–
15–16	0.76	381	49	–	–
19–20	0.76	351	27	–	–
24–25	0.79	478	42	–	–
27–28	0.82	330	37	–	–
29–30	0.82	471	39	–	–
29–30	0.82	585	60	–	–
31–32	0.82	443	54	–	–
31–32	0.82	482	49	–	–
34–35	0.79	237	52	–	–
39–40	0.80	342	36	–	–
44–45	0.78	233	46	–	–
49–50	0.71	236	37	–	–
52–53	0.67	160	36	–	–

pounds are still accumulating on the Palos Verdes shelf, despite the fact that known sources of DDTs from the Whites Point outfall were apparently eliminated in the early 1970s. A sediment redistribution mechanism, whereby contaminants in shallower sediments are periodically winnowed out and transported to deeper sediments situated further offshore, could explain apparent high concentrations and accumulation rates at the 60 m sites. Continuing outfall discharges and associated scavenging from seawater may also be significant. In addition, river washloads continue to supply many of these contaminants to the area (Inman and Jenkins, 1999; Hickey and Kachel, 2000). We therefore conclude that natural recovery has occurred to such an extent that the threat of contamination from the site is minimal. Natural recovery processes will likely continue into the future.

### Acknowledgements

We acknowledge helpful comments by John List and Susan Paulsen. We are also grateful to Dr. Glenn

Jones, Texas A&M University at Galveston, for advice and help with foraminifera identification, sorting and instrumentation used in the radiocarbon work. Radiocarbon measurements were carried out at the National Oceanographic Sciences Accelerator Mass Spectrometry Facility at the Woods Hole Oceanographic Institution. This research was supported by Montrose Chemical Corporation of California, Stauffer Management, Rhone-Poulenc, and Chris-Craft Industries.

## Appendix A

Table A1.

Table A2.

Table A3.

## References

- Adloff, J.-P., Guillaumont, R., 1993. *Fundamentals of Radiochemistry*. CRC Press, Boca Raton, pp. 167–168.
- Bacon, M.P., Van der Loeff, M.M.R., 1989. Removal of Th-234 by scavenging in the bottom nepheloid layer of the ocean. *Earth Planet. Sci. Lett.* 92 (2), 157–164.
- Bascom, W., 1982. The effects of waste disposal on the coastal waters of Southern California. *Environ. Sci. Technol.* 16, 226A–236A.
- Baskaran, M., Santschi, P.H., Guo, L., Bianchi, T.S., Lambert, C., 1996.  $^{234}\text{Th}$ :  $^{238}\text{U}$  disequilibria in the Gulf of Mexico: importance of organic matter and particle concentration. *Cont. Shelf Res.* 16, 353–380.
- Berelson, W.M., Hammond, D.E., 1987. In: Graves, B. (Ed.), Radon, Radium, and other Radioactivity in Ground Water. Hydrogeologic Impact and Application to Indoor Airborne Contamination. Proc. NWWA Conference, April 7–9, 1987. Lewis Publ., Somerset, NJ, pp. 271–281.
- Carry, C.W., 1996. Los Angeles Count Sanitation Districts Annual Report. Palos Verdes Ocean Monitoring, 1995.
- Crusius, J., 1992. Evaluating the mobility of  $^{210}\text{Pb}$ ,  $^{137}\text{Cs}$  and  $^{239,240}\text{Pu}$  from their distributions in laminated sediments. PhD Dissertation, Columbia University, New York.
- Drake, D.E., 1994. Results of grain size and settling analyses of sediment on the Palos Verdes Margin. Appendix D to Predictive modeling of the natural recovery of the contaminated effluent-affected sediment, Palos Verdes Margin, Southern California. Expert Report. USGS Expert Report.
- Drake, D.E., Eganhouse, R.P., 1994. Distribution of p,p'-DDE and organic carbon in two sediment samples from USGS box core 147 B3. Appendix F to Predictive modeling of the natural recovery of the contaminated effluent-affected sediment, Palos Verdes Margin, Southern California. Expert Report. USGS Expert Report.
- Drake, D.E., Cacchione, D.A., Karl, H.A., 1985. Bottom currents and sediment transport on San-Pedro Shelf, California. *J. Sediment. Petrol.* 55, 15–28.
- Drake, D.E., Sherwood, C.R., Wiberg, P.L., 1994. Predictive modeling of the natural recovery of the contaminated effluent-affected sediment, Palos Verdes Margin, Southern California. USGS Expert Report.
- Eganhouse, R.P., 1978. Hydrocarbons, free fatty acids and stable nitrogen isotopes in sewage effluent, outfall sediments and flocculents. Annual Rep. to U.S. Dept. of Energy, Bureau of Land Management. Contract no. EY-76-3-03-0034, 39 pp.
- Eganhouse, R.P., 1994. Geochemical Process Studies on the Palos Verdes Shelf. Final Draft Report to the National Oceanic and Atmospheric Administration, U.S. Geological Survey, Reston, VA, August 26.
- Eganhouse, R.P., 1996. Depositional history of sediments near a major submarine municipal wastewater outfall system. *ACS, Environ. Chem. Div. Abstr.* 36 (1), 145–148.
- Eganhouse, R.P., Kaplan, I.R., 1982. Extractable organic matter in municipal wastewaters: 1. Petroleum hydrocarbons: temporal variations and mass emission rates to the ocean. *Environ. Sci. Technol.* 16, 180–196.
- Eganhouse, R.P., Kaplan, I.R., 1988. Depositional history of recent sediments from San Pedro shelf, California: reconstruction using elemental abundance, isotopic composition and molecular markers. *Mar. Chem.* 24, 163–191.
- Eganhouse, R.P., Pontolillo, J., 2000. Depositional history of organic contaminants on the Palos Verdes Shelf, California. *Mar. Chem.* 70, 317–338.
- Eganhouse, R.P., Venkatesan, M.I., 1993. Chemical oceanography and geochemistry. In: Dailey, M.D., Persh, D.J., Anderson, J.W. (Eds.), *Ecology of the Southern California Bight. A Synthesis and Interpretation*. Univ. of California Press, Berkeley, pp. 71–189.
- Emery, K.O., 1960. *The Sea off Southern California*. Wiley, New York, 366 pp.
- Farley, K.J., 1990. Predicting organic accumulation in sediments near marine outfalls. *J. Environ. Eng.* 116 (1), 144–165.
- Folk, R.L., 1968. *Petrology of Sedimentary Rocks*. Hemphill Publishers, Austin, TX, 170 pp.
- Fuller, C., Hammond, D.E., 1985. The fallout rate of  $^{210}\text{Pb}$  on the western coast of the United States. *Geophys. Res. Lett.* 10, 1164–1167.
- Galloway, J.N., 1972. *Mans's Alteration of the Natural Geochemical Cycle of Selected Trace Metals*. PhD Dissertation, Scripps Institution of Oceanography, University of California San Diego, 143 pp.
- Gorsline, D.S., 1992. The geological setting of Santa Monica and San Pedro Basins, California Borderland. *Prog. Oceanogr.* 30, 1–36.
- Guo, L., Santschi, P.H., 1997. Isotopic and elemental characterization of colloidal organic matter from the Chesapeake Bay and Galveston Bay. *Mar. Chem.* 59, 1–15.
- Guo, L., Santschi, P.H., 2000. Sedimentary sources of old high molecular weight dissolved organic matter from the ocean

- margin benthic nepheloid layer. *Geochim. Cosmochim. Acta* 64, 651–660.
- Guo, L., Santschi, P.H., Cifuentes, L.A., Trumbore, S., Southon, J., 1996. Cycling of dissolved organic matter in the Middle Atlantic Bight as revealed by carbon isotopic ( $^{13}\text{C}$ ,  $^{14}\text{C}$ ) signatures. *Limnol. Oceanogr.* 41, 1242–1252.
- Gustafsson, Ö., Gschwend, P.M., 1998. The flux of black carbon to surface sediments on the New England continental shelf. *Geochim. Cosmochim. Acta* 62, 465–472.
- Hedges, J.I., Stern, J.H., 1984. Carbon and nitrogen determinations of carbonate-containing solids. *Limnol. Oceanogr.* 29, 657–663.
- Hickey, B.M., Kachel, N.B., 2000. The influence of river plumes in the Southern California Bight. *Cont. Shelf Res.* in press.
- Inman, D.L., Jenkins, S.A., 1999. Climate change and the episodicity of sediment flux of small California rivers. *J. Geol.* 107 (3), 251–270.
- Inman, D.L., Jenkins, S.A., Masters, P.M., 2000. Budget of sediment and fate of DDT at the ocean edge of the Southern California Bight. A technical report with combined database and publishable findings. Technical report submitted as an expert report in United States of America, et al. v. Montrose Chemical Corporation of California, et al., CV 90 3122-AAH(JRx).
- Jones, G.A., 1994. Holocene climate and deep-ocean circulation changes-evidence from Accelerator Mass Spectrometer radiocarbon dated argentine basin (SW Atlantic) mudwaves. *Paleoceanography* 9 (6), 1001–1016.
- Karl, H.A., 1976. Processes influencing transportation and deposition of sediment on the continental shelf, Southern California, PhD Thesis (Geological Sciences), University of Southern California, 331 pp.
- Karl, H.A., 1994. High-resolution seismic-reflection profiling survey of the Palos Verdes shelf and vicinity. Quaternary sediment thickness and accumulation rate. Appendix K to: Predictive Modeling of the Natural Recovery of the Contaminated Effluent-Affected Sediment, Palos Verdes Margin, Southern California. Expert Report, U.S. Geological Survey.
- Kayen, R.E., Hein, J.R., Wong, F.L., 1994. Contribution of the Portuguese Bend landslide of the recent accretion of sediment on the Palos Verdes shelf, Southern California. Appendix I, “Predictive modeling of the natural recovery of the contaminated effluent-affected sediment, Palos Verdes margin, Southern California”. Expert Report, U.S. Geological Survey.
- Lee, H.J., 1994. The Distribution and Character of Contaminated Effluent-Affected Sediment, Palos Verdes Margin, Southern California, USGS Expert Report.
- List, E.J., Paulsen, S.C., 2000. In situ biodegradation rates of p,p'-DDE in the sediments of the Palos Verdes Shelf, Southern California: An analysis of field evidence. Technical report submitted as an expert report in United States of America, et al. v. Montrose Chemical Corporation of California, et al., CV 90 3122-AAH(JRx).
- Logan, B.E., Steele, J.A., Arnold, R.G., 1989. Computer-simulation of DDT distribution in Palos-Verdes Shelf sediments. *J. Environ. Eng.* 115 (1), 221–238.
- McNichol, A.P., Osborne, E.A., Gagnon, A.R., Fry, B., Jones, G.A., 1994. TIC, TOC, DIC, DOC, PIC, POC — Unique aspects in the preparation of Oceanographic samples for  $^{14}\text{C}$  — AMS. *Nucl. Instr. Methods in Physics Res. Section B* 92, 162–165.
- Myers, E.P., 1974. The concentration and isotopic composition of carbon in marine sediments affected by a sewage discharge. PhD Dissertation, Calif. Inst. of Technol., Pasadena, CA, 179 pp.
- Niedoroda, A.W., Swift, D.J.P., Reed, C.W., Stull, J.K., 1996. Contaminant dispersal on the Palos Verdes continental margin: III. Processes controlling transport, accumulation and re-emergence of DDT-contaminated sediment particles. *Sci. Total Environ.* 179, 109–133.
- Oktay, S.D., Santschi, P.H., Moran, J.E., Sharma, P., 2000. The  $^{129}\text{I}$  iodine bomb pulse recorded in Mississippi river delta sediments: results from isotopes of I, Pu, Cs, Pb, and C. *Geochim. Cosmochim. Acta* 64 (6), 989–996.
- Paulsen, S.C., List, E.J., Santschi, P.H., 1999. Modeling variability in  $^{210}\text{Pb}$  and sediment fluxes near the Whites Point outfalls, Palos Verdes shelf, California. *Environ. Sci. Technol.* 33 (18), 3077–3085.
- Quensen III, J.F., Mueller, S.A., Jain, M.K., Tiedje, J.M., 1999. Reductive dechlorination of DDE to DDMU in marine sediment microcosms. *Science* 280, 722–724.
- Ravichandran, M., Baskaran, M., Santschi, P.H., Bianchi, T.S., 1995a. History of trace metal pollution in Sabine–Neches estuary, Beaumont, Texas. *Environ. Sci. Technol.* 29, 1495–1503.
- Ravichandran, M., Baskaran, M., Santschi, P.H., Bianchi, T.S., 1995b. Geochronology of sediments of Sabine–Neches Estuary, Texas. *Chem. Geol.* 125, 291–306, (Isotope Geoscience).
- Renner, R., 1998. “Natural” remediation of DDT, PCBs debated. *Environ. Sci. Technol.* 32 (15), 360A–363A.
- Robbins, J.A., McCall, P.L., Fisher, J.B., Krezoski, J.R., 1979. Effect of deposit feeders on migration of  $^{137}\text{Cs}$  in lake sediments. *Earth Planet. Sci. Lett.* 42, 277–287.
- Santschi, P.H., Honeyman, B.D., 1989. Radionuclides in aquatic environments. *Radiat. Phys. Chem.* 34 (2), 213–240.
- Santschi, P.H., Li, Y.-H., Bell, J., Trier, R.M., Kawtaluk, K., 1980. Plutonium in the coastal marine environment. *Earth Planet. Sci. Lett.* 51, 248–265.
- Santschi, P.H., Adler, D., Amdurer, M., 1983. The fate of particles and particle-reactive trace metals in Sea Water. In: Wong, C.S., Boyle, E., Bruland, K., Burton, J.D., Goldberg, E.D. (Eds.), *Trace Metals in Sea Water*. Plenum Press, New York, pp. 331–350.
- Santschi, P.H., Bollhalder, S., Farrenkothen, K., Lueck, A., Zingg, S., Sturm, M., 1988. Chernobyl radionuclides in the environment: tracers for the tight coupling of atmospheric, terrestrial and aquatic geochemical processes. *Environ. Sci. Technol.* 22, 510–516.
- Santschi, P.H., Bollhalder, S., Zingg, S., Lueck, A., Farrenkothen, K., 1990. The self-cleaning capacity of surface waters after radioactive fallout. Evidence from European waters after Chernobyl, 1986–1988. *Environ. Sci. Technol.* 24, 519–527.
- Santschi, P.H., Allison, M., Asbill, S., Perlet, A.B., Cappellino, S., Dobbs, C., McShea, L., 1999. Sediment transport and Hg

- recovery in Lavaca Bay, as evaluated from radionuclide and Hg distributions. *Environ. Sci. Technol.* 33, 378–391.
- Santschi, P.H., Guo, L., Wen, L.-S., 2000a. Box coring artifacts in sediments affected by a waste water outfall. *Mar. Pollut. Bull.* in press.
- Santschi, P.H., Wen, L.S., Guo, L., 2000b. Transport and diagenesis of trace metals and organic matter in Palos Verdes shelf sediments affected by a sewage outfall. *Mar. Chem.* 73 (2).
- Schwalbach, J.R., Gorsline, D.S., 1985. Holocene sediment budgets for the basins of the California continental borderland. *J. Sediment. Petrol.* 55, 829–842.
- Sommerfield, C.K., Nittrouer, C.A., 1999. Modern accumulation rates and a sediment budget for the Eel shelf: a flood-dominated depositional environment. *Mar. Geol.* 154, 227–241.
- Sommerfield, C.K., Nittrouer, C.A., Alexander, C.R., 1999. Be-7 as a tracer of flood sedimentation on the northern California continental margin. *Cont. Shelf Res.* 19, 335–361.
- Stull, J.K., Haydock, C.I., Smith, R.W., Montagne, D.E., 1986. Long-term changes in the benthic community on the coastal shelf of Palos Verdes, Southern California. *Mar. Biol.* 91, 539–551.
- Stull, J.K., Swift, D.J.P., Niedoroda, A.W., 1996. Contaminant dispersal on the Palos Verdes continental margin: I. Sediment and biota near a major California wastewater discharge. *Sci. Total Environ.* 179, 73–90.
- Sweeney, R.E., Kalil, E.K., Kaplan, I.R., 1980. Characterization of domestic and industrial sewage in Southern California coastal sediments using nitrogen, carbon, sulphur and uranium tracers. *Mar. Environ. Res.* 3, 225–243.
- Swift, D.J.P., Stull, J.K., Niedoroda, A.W., Reed, C.W., Wong, G.T.F., 1996. Contaminant dispersal on the Palos Verdes continental margin: II. Estimates of the bioturbation coefficient,  $D_b$ , from composition of the benthic infaunal community. *Sci. Total Environ.* 179, 91–107.
- Van Cappellen, P., Santschi, P.H., Cai, W.-J., Wen, L.-S., 2000. Organic matter degradation and bioirrigation in marine sediments impacted by wastewater outfall (Palos Verdes Shelf, Southern California Bight). *Mar. Chem.*, to be submitted.
- Van Metre, P.C., Wilson, J.T., Callender, E., Fuller, C.C., 1998. Similar rates of decrease of persistent, hydrophobic and particle-reactive contaminants in riverine systems. *Environ. Sci. Technol.* 32, 3312–3317.
- Wan, G.J., Santschi, P.H., Sturm, M., Farrenkothen, K., Werth, E., Schuler, C., 1987. Natural ( $^{210}\text{Pb}$ ,  $^7\text{Be}$ ) and fallout ( $^{137}\text{Cs}$ ,  $^{239,240}\text{Pu}$ ,  $^{90}\text{Sr}$ ) radionuclides as geochemical tracers of sedimentation in Greifensee, Switzerland. *Chem. Geol.* 63, 181–196.
- Wheatcroft, R.A., Martin, W.R., 1994. Solid-phase bioturbation processes on the Palos Verdes shelf. Appendix E, to: Predictive modeling of the natural recovery of the contaminated effluent-affected sediment, Palos Verdes Margin, Southern California. WHOI Expert Report.
- Wheatcroft, R.A., Martin, W.R., 1996. Spatial variation in short-term ( $^{234}\text{Th}$ ) sediment bioturbation intensity along an organic-carbon gradient. *J. Mar. Res.* 54, 763–792.
- Wheatcroft, R.A., Sommerfield, C.K., Drake, D.E., Borgeld, J.C., Nittrouer, C.A., 1997. Rapid and widespread dispersal of flood sediment on the northern California margin. *Geology* 25, 163–166.
- Williams, P.M., Robertson, K.J., Soutar, A., Griffin, S.M., Druffel, E.R.M., 1992. Isotopic signatures ( $^{14}\text{C}$ ,  $^{13}\text{C}$ ,  $^{15}\text{N}$ ) as tracers of sources and cycling of soluble and particulate organic matter in the Santa Monica Basin, California. *Prog. Oceanogr.* 30, 253–290.
- Wong, F.L., 1994. Heavy-mineral provinces of the Palos Verdes area, southern California. In: Predictive modeling of the natural recovery of the contaminated effluent-affected sediment, Palos Verdes margin, southern California, Appendix J, Expert Report for the Southern California Damage Assessment Study, October, 1994, 50 pp.
- Wong, K.M., Jokela, T.A., Eagle, R.J., Brunk, J.L., Noshkin, V.E., 1992. Radionuclide concentrations, fluxes, and residence times at Santa Monica and San Pedro Basins. *Prog. Oceanogr.* 30, 353–391.
- Young, D.R., McDermott, D.J., Heesen, T.C., Jan, T.K., 1975. Pollutant inputs and distributions off Southern California. In: Church, T.M. (Ed.), *Marine Chemistry in the Coastal Environment*. American Chemical Society, Washington, DC, pp. 424–439. ACS Symp., Series 18.
- Zeng, E.Y., Venkatesan, M.I., 1999. Dispersion of sediment DDTs in the coastal ocean off southern California. *Sci. Total Environ.* 229, 195–208.
- Zeng, E.Y., Yu, C.C., Tran, K., 1999. In situ measurements of chlorinated hydrocarbons in the water column off the Palos Verdes Peninsula, California. *Environ. Sci. Technol.* 33 (3), 392–398.